A SELF CORRECTIVE VORTEX FLUXING METHOD FOR VISCOUS FLUID STRUCTURE INTERACTION PROBLEMS

BY

VEDANT DUBEY

THESIS

Submitted in partial fulfillment of the requirements
for the degree of Master of Science in Aerospace Engineering
in the Graduate College of the
University of Illinois at Urbana-Champaign, 2018

Urbana, Illinois

Adviser:

Assistant Professor Mattia Gazzola

Abstract

Computational Fluid Dynamic Solvers for flow structure interaction problems rely on a delicate treatment of fluid and grid properties close to the boundary. Although such an approach is accurate, it proves to be inflexible when applied to complex deforming geometries. Here we combine remeshed vortex methods with a panel method to design a new Vortex Fluxing scheme that uses no special treatment of flow properties at the boundary. It was found that the panel method is capable of correcting any spurious vorticity flux into the wall during the no slip boundary application. This enables highly accurate, robust Direct Numerical Simulations by relaxing the need for small timesteps and allowing the use of coarse regular computational grids. The methodology was validated for rigid, rotating and deforming bodies. ....

Table of Contents

Chapter 1

Introduction

Vortex particle methods have proved to be a viable alternative to Finite Volume Methods (FVM) and Finite Element methods (FEM) for studying fluid structure problems. Unlike FVM/FEM methods vortex particle methods do not rely on body fitted grids for accuracy and are not constrained by the severe CFL condtion. The CFL condition is replaced by the Lagrangian CFL condition that allows the user to take significantly larger time steps for a given grid resolution. Moreover vortex particle methods provide compact support, which provides higher computational efficiency by solving only where vorticity is non-zero. Over the years,two distinct vortex particle methods have evolved namely : Brinkmann Penalization [1] [2] and Vortex Panel-Particle Method [3] and [4].

The Brinkmann Penalization method provides robustness and flexibility in dealing with complex deforming geometries with no special treatment close to boundary necessary. This advantage has been utilized by Gazzola [1] to study flow around self propelling deforming bodies on a regular Cartesian grid. However Brinkmann Penalization cancels the LCFL large timestep advantage that is the core strength of vortex methods. The large forcing of flow only restricts the user to small time steps of order ($1e^{-4}$-$1e^{-5}$) to maintain stabilty.

Vortex-Panel particle methods pose as a viable alternative by preserving the LCFL advantage and taking larger timesteps ($1e^{-2}$) .However most previous work has been restrictive in the robustness and flexibility of this method to general geometries. For example, the Komoutsakos [5] utilized a body fitted particle grid combined with special stencils close to boundary for studying cylinder flows. Eldredge [6] used body aware particle strength exchange schemes along with close refinement at walls to ensure a fresh layer of vortex particles appear around body at each timestep. Ploumhans [3] uses particle imaging close to boundary to cancel spurious vorticity flux and reflection of particles at boundary to prevent convective leakages. The latter approach is aphysical and causes noise in the force calculation.

Thus special treatment in the above methods detracts from the robustness and flexibility of the vortex panel methods. It is desirable is to combine the advantages of both the dominant particle methods .The resulting solver must be robust and flexible with no special treatment at wall with large timesteps.

Recent studies point towards the fact that vortex panel methods are inherently self corrective and special treatment close to walls might not be necessary.

The motivation of the current research, stems from three different preliminary findings. Ploumhans [7] implemented a Straight forward Particle Redistribution Scheme (SF) where symmetric remeshing kernels were used for symmetric flow past an impulsively started cylinder at Re=300 ,500,1000 and asymmetric flow past a square at Re 100. It was found that any vorticity leaked into the body during remeshing, provided the panel solver with an artificial boundary condition that the vortex sheet algorithm corrected afterwards by injecting the right amount of vorticity into the flow. It is expected that for symmetric cylinder flow an equal amount of positive and negative vorticity leaked into the body .Thus in this special case,vorticity was implictly conserved . However in the case of asymmetric flow past a square,a non zero amount of vorticity leaks into the body during remeshing that is account for by a modification of the Kelvin Circulation theorem For the case of an asymmetric flow, Eldredge [6] utilized vortex particle method to study flow past flapping two dimensional wings. During the remeshing step, a similar body ignorant interpolation scheme was used which allows vorticity to leak into the body. A modified Kelvin Circulation Theorem was used to correct for nonzero vorticity leaked into the body. The algorithm utilized careful special treatment of vorticity layer next to the body during all other steps of the algorithm including diffusion and convection and used Particle Strength Exchange . An encouraging comment by Cottet and Winckelmans [8] indicated that use of body unaware diffusion and remeshing techniques introduces spurious vorticity flux into the body, that the panel method is designed to correct on its own. In other words symmetric diffusion and remeshing kernels one can rely on the panel method to correct any mistakes close to the boundary. However, a validation for such a body unaware scheme was not given.

All three studies point to the possibilty of relying on the self corrective aspect of the vorticity flux step to remove any special treatment of flow close to the wall. This proves advantageous when extending the current method to complex geometries such as a fish where body aware (one sided) interpolation schemes become cumbersome and difficult.

Our method differs from the above implementations by extending and validating this assumption. We use symmetric diffusion and remeshing stencils which effectively leak vorticity into the body. In a physical flow the global sum of vorticity must be conserved. In order to account for the vorticity lost into the body we utilize a modified Kelvin Ciculation theorem. Any vorticity that enters in to the body must find its way back into the flow at the next timestep. With this modification the process then relies completely on the vorticity flux step ability to correct any spurious vorticity fields. Thus we remove the need for any special treatment of the grid close to walls in the form of body fitted grids or biased stencils. We have also removed the

need for using Particle Strength exchange and utilized finite difference method for the diffusion step. This increases the computational efficiency of the diffusion step due to circumventing the lower computational cost in tracking particles in space incurred by PSE. At the same time, the current method comes under the classification of Vortex in Cell methods that lend themselves better to parallelization as compared to the previous predominantly vortex particle methods.

Chapter 2

Panel method: The core of the Vortex Fluxing solver

In this chapter we introduce the vortex panel method,a well known method to solve inviscid aerodynamic flows. We show how the panel method can be extended to viscous applications.

2.1 Origin of Panel methods

In any viscous flow, the boundary can be considered a source of vorticity. The shedding of this vorticity leads to the formation of a viscous boundary on the surface of the body. However as the Reynolds number is increased and the viscosity tends to zero,this boundary layer becomes infinitely thin. In such a case it is a reasonable assumption to conclude that vorticity is "attached" to the surface geometry. With this assumption, an inviscid flow can be used to simulate the flow dynamics of a system. In order to solve for the vortex sheet strength -two types of constraints can be applied to the flow,namely no slip and no throughflow.

2.2 The no slip and no throughflow boundary condition

For a viscous bounded simulation, the no slip boundary condition is applied at the wall to create a boundary layer. The no slip equation can be written as follows:

$$u.s = u_b.s \tag{2.1}$$

Where u_b is the velocity at a point on the surface of the body and s denotes the tangent to the surface. While applying the nboundary condition one can also apply no throughflow conditon written as

$$u.n = u_b.n \tag{2.2}$$

Here n denotes the normal vector at the surface of the body. The no throughflow boundary condition is used most popularly in panel methods [9] to simulate inviscid flows whereas the no slip condition has direct

application in viscous flows.

2.3 Computing Vortex Sheet Strengths

The procedure for applying the no slip condition requires the computation of the fluid velocity on the surface.

In order to compute the fluid velocity,a Heimholtz Decomposition of the flow can be carried out similar to inviscid flows. At each point on the surface of the body, velocity can be computed by splitting the contributions from different sources as follows:

$$u = u_\infty + u_b + u_\omega + u_\gamma \tag{2.3}$$

Here u_∞, u_ω refer to the velocity induced by farfield velocity and the vortex particles in the fluid respectively. The computation of the vortex particle influence is speeded up by the use of a Fast Multipole Solver. u_b refers to the influence of the kinematics of the body on the surrounding flow and is discussed in Chapter 3. This influence is independent of the fluid flow. Since no slip implies $u.s = u_{body}.s$,the only unknown in the above equation is u_γ which refers to the velocity induced by the vortex sheet. We can thus reformulate the no slip equation as:

$$u_{body} = u_{ext} + u_s - \frac{\gamma(s)}{2} + \oint_{Body} K \times \gamma(s) ds \tag{2.4}$$

Where u_{ext} denotes the influence of the fluid vorticity and farfield and K refers to the velocity kernel of influence of the vortex sheet. u_s refers to the influence of the body towards convection. The term $\frac{\gamma}{2}$ is the influence of a vortex sheet upon its own centre which is non singular. This equation is known as Friedholm's integral equation of the second kind. The above equation states that the sum of all the influences to the velocity on the Right Hand Side (RHS) must equal the local surface velocity. It is important to state that the vortex sheet is an infinitely thin sheet that cancels the slip **below** the vortex sheet and **above** the surface of the body. The only unknown in the given equation is the vortex strength distribution $\gamma(s)$ as a function of the surface contour. In order to find γ we discretize the continous vortex sheet on the surface into discrete panels.

It is possible to express each panel as a constant, linear or cubic vortex sheet strength distribution. In our formulation we utillize the constant sheet strength approximation in order to solve the no slip equation.

2.4 The constant Strength Panel

The constant strength vortex panel method discretizes the vortex sheet strength distribution $\gamma(s)$ into straight line elements of piecewise constant strength. The midpoint of each panel is reffered to as the colllocation point. We compute the vortex sheet strength by applying the no slip condition at the collocation point of each panel given by equation (2.4). Figure 3(a) represents the influence of panel j on panel i in the velocity contribution.

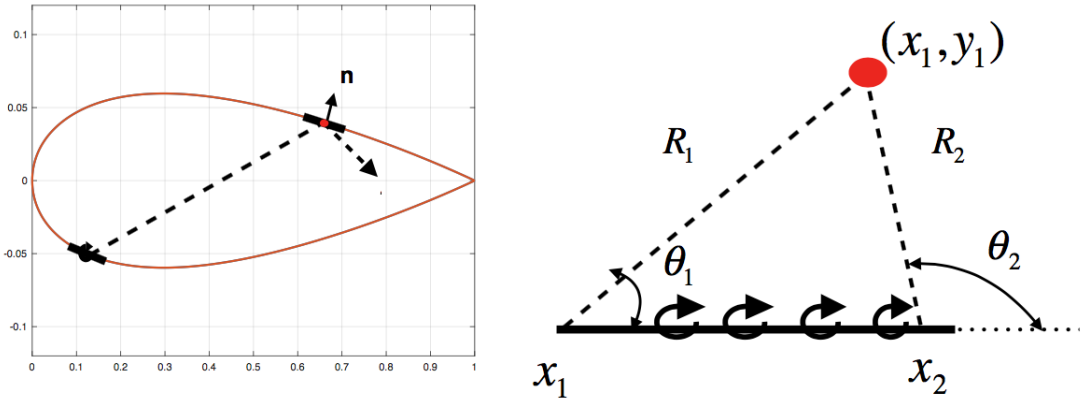

Figure 2.1: The influence of a vortex panel at a given collocation point

Our methodology follows the development of Katz and Plotkin [9] in order to find the velocity induced at any point by the vortex sheet. In order to compute the velocity induced at the i^{th} collocation point we transform to the local coordinate system of panel j such that x_1 becomes the new origin.
Within this frame of reference shown in Fig 3 (b), the velocity induced at the new coordinates of i^{th} panel a (x_1, y_1) can be written as:

$$u' = \frac{1}{2\pi}(\theta_2 - \theta_1) \tag{2.5}$$

$$v' = \frac{1}{2\pi}\log\left(\frac{R_2}{R_1}\right) \tag{2.6}$$

Where u' and v' are the velocity induced at the i^{th} collocation point in the x and y direction respectively. Once these velocites are found we rotate the velocities back to the original coordinate system usng the transformation:

$$\begin{bmatrix} u \\ v \end{bmatrix} = \begin{bmatrix} \cos\theta & -\sin\theta \\ -\sin\theta & \cos\theta \end{bmatrix} \begin{bmatrix} u' \\ v' \end{bmatrix} \tag{2.7}$$

With the velocities u and v in the global coordinate system we can compute the slip induced by the j^{th}

panel on the i^{th} collocation point as:

$$u_{slip(i,j)} = u\cos\theta + v\sin\theta \tag{2.8}$$

Which can be rewritten as:

$$u_{slip(i,j)} = A_{i,j}\gamma_j \tag{2.9}$$

Where $A_{i,j}$ is the influence coefficient of the j^{th} panel on th i^{th} collocation point. We can represent the no slip equation (2.4) as a matrix system with mutual influence coefficients which can be inverted to compute the piecewise vortex sheet strengths for m individual panels. Besides satisfying the no slip conditions,the sum of the vortex sheets must also conserve vorticity circulation by the Kelvin Circulation theorem.

$$\begin{bmatrix} A_{1,1} & A_{1,2} & . & . & . & A_{1,m} \\ A_{2,1} & . & & & & \\ . & & . & & & \\ . & & & . & & \\ . & & & & . & \\ A_{m,1} & . & . & . & A_{m-1,m} & A_{m,m} \\ ds_1 & ds_2 & . & . & . & ds_m \end{bmatrix} \begin{bmatrix} \gamma_1 \\ \gamma_2 \\ . \\ . \\ . \\ . \\ \gamma_m \end{bmatrix} = \begin{bmatrix} RHS_1 \\ RHS_2 \\ . \\ . \\ . \\ RHS_m \\ \Gamma_{correction} \end{bmatrix} \tag{2.10}$$

The Right Hand side denotes all other contributions to slip besides the vortex sheet known beforehand. The first m equations mentioned are the no slip equations at each of the m collocation points and the last $(m+1)^{th}$ equation is the conservation of circulation give by the Kelvin Circulation theorem which is explained in section 2.6.

2.5 The Linked Kinematic Boundary Condition

In the previous section, the no slip boundary condition was applied to solve for the vortex sheet strengths. A physical flow must satisfy both no slip and no throughflow simaltenously at the boundary. Spallart [10] mathematically proved that application of no slip automatically applies ensures no throughflow in the context of vortex methods. This abilty to satisfy both conditions simaltenously has been reffered to by Barba and Cooper [11] as the **linked kinematic boundary condition.**

Komoutsakos [4] and Pepin[12] have utillized this linked boundary application by only using the no slip boundary condition in the algorithm and leaving out no throughflow correction.

If no slip does indeed give no throughflow, the flow should correspondingly model the inviscid panel method flowfield as long as the vortex sheets remain attached to the body . To verify this, we study the flowfield past a cylinder composed of Radius 1 unit with a freestream velocity $U_\infty = 1$ past it in the x direction . The cylinder is composed of 200 panels with the strengths calculated to satisfy no slip using **??** .The velocity induced within a box of [-2,2] units made of a mesh of [200,200] points is computed using the analytical velocity induced by the constant strength panels. The velocity solution is then compared with the analytical solution for inviscid flow past a cylinder of the same radius.

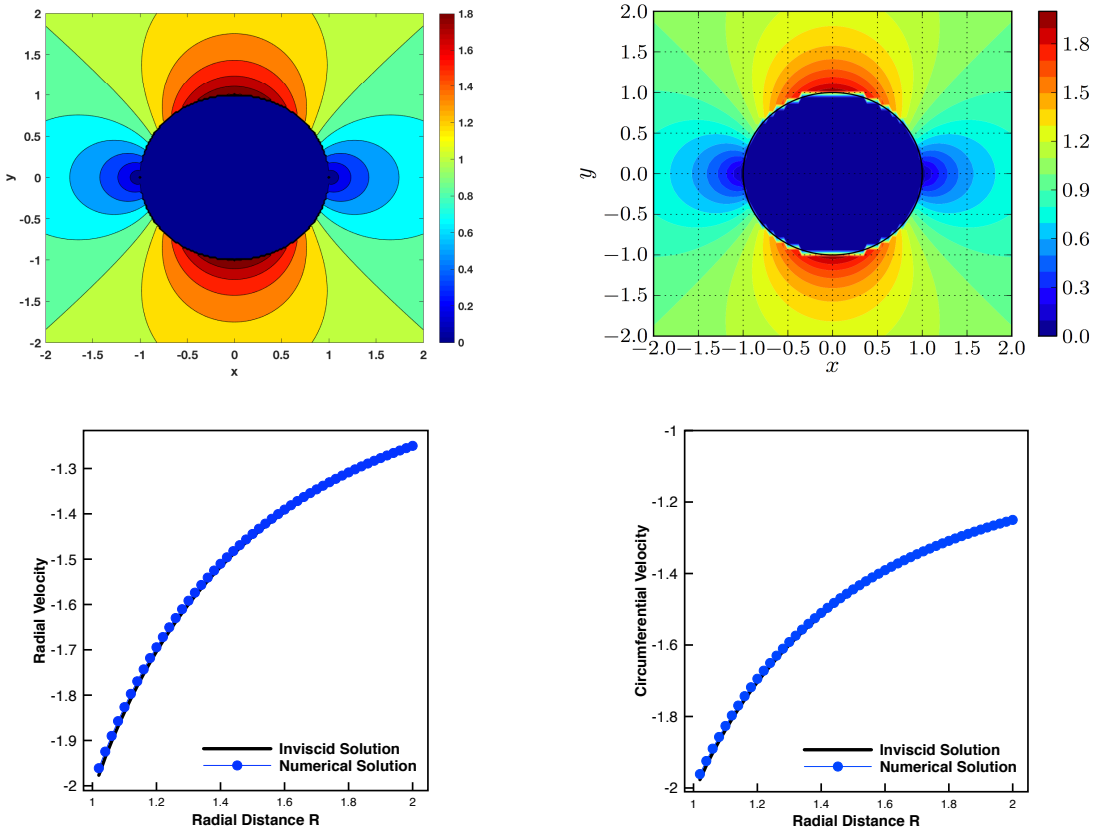

Figure 2.2: (Top left) Our solution for inviscid flow past a cylinder (Top right) Potential Solution given by Mackinathan (Botton left) Comparision of numerical Radial velocity at $\theta = 45$ with inviscid solution (Bottom right) Comparision of Circumferential Velocity at $\theta = 90$ with inviscid solution

We observe in figure 2.7 that the numerical solution solving for no slip does indeed replicate the inviscid no throughflow solution given by Mackinathan [13].There is a small discrepancy in the maximum value which can be explained by the vortex sheet velocity kernel becoming a singularity as the mesh resolution is increased such that the closest particle to the wall shortens its distance to the wall. The radial velocity profile at $\theta = 45$ and the circumferential velocity profile at $\theta = 90$ respectively for the analytical no throughflow solution matches well with the numerical solution solving for no slip.

Thus in our formulation we only apply the no slip boundary condition. The above boundary condition applies no slip to calculate vortex sheet. However, there is a direct link between the application of no slip and no through flow boundary condition.

While this is true, from a mathematical standpoint, the argument has rarely been validated numerically. Spallart [10] proves that for the implicit application of the no penetration boundary condition, the body must have a finite area. This assumption clearly fails for the case of a flat plate. Thus it is expected that the no penetration condition is only approximately satisfied numerically when the thickness of a body is decreased relative to grid spacing. The error in satisfying no penetration was within 1% of local velocity for a bluff body, whereas iterative fluxing within the no slip substep eliminates this error down to 0.01 %. Infact for sharp trailing edge geometries such as airfoils the GMRES Vortex Sheet Calculation during the no slip step gives an infinite value of throughflow at the singularity.

It was however found, that for non singular geometries, the panel method is capable of correcting any spurious vorticity fluxes by convective leakage into the body on its own thus removing the need to satisfy the no penetration condition strictly.

2.6 Kelvin Circulation Theorem and Self Correction

The total circulation created within a fixed control volume must remain constant with time. This can be written as:

$$\frac{d\Gamma}{dt} = 0 \tag{2.11}$$

Where Γ denotes circulation. This expression is known as the Kelvin Circulation theorem. If the system has no vorticity at initial conditions then the circulation of the body and fluid msut sum to zero at all times.

$$\Gamma_{body} + \Gamma_{fluid} = 0 \tag{2.12}$$

While solving for no slip on all N panels in section 2.4 we must also satisfy this additional $(N+1)^{th}$ constraint to conserve circulation by a least squares emthod. This constraint is used for the conservation of circulation to make sure the net circulation of the flow and body sums to zero. In section 2.4 , we solve for no slip and apply the extra constraint on the vortex sheet strengths as follows:

$$\oint_{Body} \gamma(s)ds = \Gamma_{correction} \tag{2.13}$$

Here $\Gamma_{correction}$ is the correct sum of the vortex sheet strengths such that vorticity is conserved within the flow.This value has two components which are used to adjust the vortex sheet strengths.

$$\Gamma_{correction} = \Gamma_{rot} + \Gamma_{leak} \tag{2.14}$$

Γ_{rot} is the correction by virtue of body rotation. Kelvn Circulation theorem specifies that the sum of the vorticity due to the vorticity by body cumulative rotation and the flow must equal zero at all times for vorticity to be conserved at the n^{th} timestep.

$$\oint_{Body} n \times u^n_{body} ds + \int_{V_{fluid}} \omega^n dA = 0 \tag{2.15}$$

Stated in alternative way we can specify Γ_{Rot} as:

$$\Gamma_{Rot} = \oint_{Body} n \times u^n_{body} ds - \oint_{Body} n \times u^{n+1}_{body} ds \tag{2.16}$$

Similarily Γ_{leak} is the sum of the cumulative circulation leaking into the body over a timestep. This vorticity must find its way back into the fluid in order to conserve circulation otherwise the solution becomes aphysical.

At the heart of the self corrective solver, the Γ_{leak} corrects any mistakes made by the solver close to the wall boundary as will be explained in Chapter 3. Since the number of equations is grater than m, the above set of equatons is solved by using a least squares-approach.

While the above formulation was proposed as the solution for small leakages into the body, an alternate formulation given by Ploumhans and Winckelmanns [3]was found to work well for highly asymmetric flows.

$$\oint_{Body} \gamma(s) ds + \sum_{Fluid} \Gamma_{particles} = -2\Omega(t + \Delta t) A_b \tag{2.17}$$

The above equation specifies that the sum of total circulation of the particles and vortex sheet on the body must exactly cancel the circulation of the body at the next timestep. This is important as in the next step the vortex sheet is released to sorrounding particles and becomes the net change in fluid circulation. This expression valid for a rigid body is mathematically identical to equation (2.12) However, it is found to work well for identical simulations running with the only modification to kelvin circulation theorem stated above with Γ_{lost} formulation giving the aphysical result. Eldredge utillzied the previous formulation for occasional remeshing thus it is expected to not work in highly asymmetric flow cases. This is explained by the fact that expression (2.14) rigidly imposes conservation of circulation by directly including the sum of circulation

of the fluid whereas expressions (2.12) and (2.13) only includes the body circulation and leakage and is thus prone to numerical errors accumulating in the fluid over time leading to non zero circulation. The formulation 2.17 conserves circulation accurately based on flow particles. For highly asymmetric flows, it is preferred to apply the circulation conservation as a rigid constraint in the form of Lagrange Multipliers.

2.7 Fluxing of the vortex sheet to surrounding particles

In a panel method, as previously shown the vortex sheets remains "attached" to the surface. However, in real viscous flows, the surface of the body acts as a continous source of vorticity entering into the surrounding flow through the formation of a boundary layer. It is thus clear, that in order to simulate viscous flows, a way to release this vorticity into the surrounding flow must be incorporated. Once the vorticity is fluxed into the surrounding flow, the no slip condition is satisfied. Panels methods enable the formation of a viscous boundary layer by releasing the attached vorticity to the surrounding flow. This is the most important distinction between inviscid panel methods and the vortex methods.

Chorin [14] first developed a way of releasing the vorticity into the surrounding flow. After computing vortex sheet strength needed to cancel slip, the discrete vortex panel is broken down into finite number of vortices and released into the flow using the Random Walk Method (RWM) at an offset distance $\sqrt{vt}$ proportional to diffusion distance. This method multiplies the total no of particles within the flow at each time step thus growing the computational time after each step. An alternative developed by Gazzola et al [1] is the Brinkmann Penalization condition.In this method the fluid is forced by using the modified vorticity streamfunction formulation.

While this formulation works well for deforming bodies, the timestep drastically reduces to maintain stabilty due to the large forcing constant needed to properly impose the rigidity of the body.

A fluxing scheme developed by Komoutsakos [4] allows the analytical diffusion of vorticity from the surface of the body by specifying the vorticity flux at each time step using the Neumann Boundary Condition for flux.

$$\frac{\gamma}{\Delta t} = -v\frac{\partial \omega}{\partial n} \tag{2.18}$$

The flux can be obtained analytically by treating the vortex sheet fluxing as the diffusion of heat from a constant temperature panel to a semi infinite plane. While Komoutsakos utilize a body fitted grid, it is desirable to want the vorticity to be fluxed onto a fixed Cartesian grid in order to enhance the robustness

of the solver. The most useful scheme beneficial to this study was the general scheme which is conservative over a non body conforming grid given by Ploumhans [7].

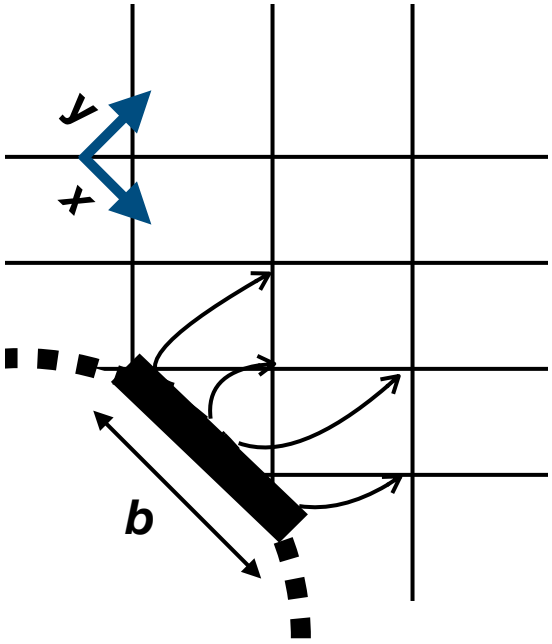

Figure 2.3: Fluxing the attached vorticity to sorrounding cartesian grid from an individual panel on the body

The analytical flux formulation for calculating the circulation released from an individual panel to sorrounding grid is given by:

$$\frac{d\Gamma}{dt} = \frac{\gamma}{\Delta t}\left(erfc(s)_{(x+h/2)/\sqrt{4v\Delta t}}^{(x-h_l/2)/\sqrt{4v\Delta t}}\right)\sqrt{v\Delta t}\left[\left(ierfc(s)_{(y+b/2+h/2)/\sqrt{4v\Delta t}}^{(y-b/2-h/2)/\sqrt{4v\Delta t}}\right) - \left(ierfc(s)_{(y+b/2+h/2)/\sqrt{4v\Delta t}}^{(y+b/2-h/2)/\sqrt{4v\Delta t}}\right)\right] \tag{2.19}$$

As shown in Figure 2.7 a panel of length b adds a circulation $d\Gamma$ to a location (x, y) on the cartesian grid in the local coordinate system of the panel. Thus the algorithm transforms to the local cooridnate frame of each panel such that the x axis lies along the panel length and distributes vorticity to a radius of $\sqrt{10v\Delta t}$. The contribution to circulation of each panel rapidly dies within this radius to zero. Here h_l denotes the spacing parameter specified by Ploumhans equal to $2h$ if within half a cell spacing of body and h otherwise. This parameter is used to adjust for the fact that the discretized size of a vortex particle within half a cell spacing is less than h^2 on account of intersection with body. The formulation in 2.19 perfectly conserves the total circulation when fluxed to a continuous analytical domain. Since the cartesian grid is irregularly spaced with respect to the panel, a small discretization error is incurred in the total circulation. We correct this error by equally distributing the remaining circulation equally to all particles within the panel flux

radius .

$$\Delta\Gamma_{conserved} = \Delta\Gamma_i + \frac{\Delta\Gamma_i}{\sum\limits_{radius} (\Delta\Gamma_i)^2}(b\gamma - \sum_{radius} \Delta\Gamma_i) \tag{2.20}$$

At the end of this correction, the total circulation error was found to be of order (1e-3) of net sum of vortex sheet strengths. The given fluxing scheme was found to be more adaptable to our solver as the particles need not track or fit their location with respect to the panels. For this reason the fluxing schemes given by Komoutsakos and Shiels which are applicable to body fitted grids were not applied.

2.8 Vortex Fluxing and No slip

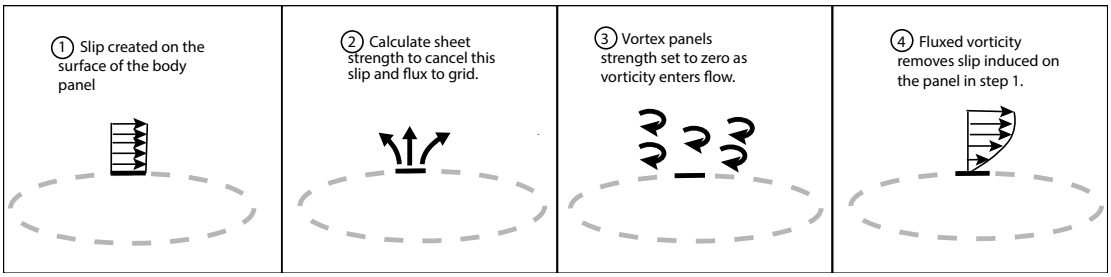

Figure 2.4: The vortex panel fluxing method procedure

As shown in the figure above we carry out the following steps to enforce no slip boundary condition:

Step (I): We compute slip on the surface of each panel using equation 2.4. The body and vortex sheet contributions are computationally inexpensive and computed directly.

Step (II): Next we compute the right hand side of the matrix given in 2.10 and invert the influence matrix to compute the vortex sheet .The influence of each panel on itself and other panels forms the influence coefficients of matrix A. The contribution of sorrounding vortex particles is carried out by setting the panel collocation points as targets and using the Fast Multipole Method(FMM) Scheme developed by Greengard et al.[15].

These contributions are then summed to form the right hand side of matrix given in 2.10. In our experience, most literature focuses on cancelling the slip yet does not specify the location where the slip is cancelled as being above or below the vortex sheet.The vortex sheet as an infinitely thin layer over the body thus one can assume it follows the body geometry with one key difference. The self induction coefficient forming the trace of matrix A is dependent on whether the slip is cancelled above or below the vortex sheet.The slip must be cancelled **below the vortex sheet** and **above the body** thus inducing an influence of $-\gamma/2$ on the body below for clockwise circulation.

Step(III): The vortex sheet once computed, is fluxed to the sorrounding cartesian grid using the heat equation solution in equation 2.19 and subsequent correction. The circulation is superimposed onto the already existing vortex particles from the previous timestep within the flow.

Step(IV): Fluxed vorticity then annihilates the slip on the surface by redistributing the vorticity around the body. This leads to the formation of a "boundary layer" as shown in figure 2.8 step 4. Thus by releasing the attached vortex sheet into the flow, we have transitioned from inviscid panel methods into the viscous regime.

2.9 Panel refinement and the Nyquist Instabilty

When a body is kept static with respect to the grid, there are no oscillations observed within the force characteristics of the solver. This is in contrast to the oscillations observed by Ploumhans at each remeshing step, when vortex particles are remeshed to the Cartesian grid. This was observed likely due to the switch from a particle method to remeshing onto a cartesian grid that causes these oscillations for a static body. However, the vortex particle method shows subgrid oscillations in its results when the body is moved inside a Cartesian grid. These oscillations were first observed by Eldredge [6] and are referred to as the Nyquist instability.

It originates at regions of high curvature as shown in the figure below. The reason for this can be summarized by looking at the "line of sight" of each panel. Each panel can see and reach a finite number of points with its diffusion radius proportional to $\sqrt{vt}$. In this case, in region of stair step configuration, a single panel reaches fewer points in regions of high curvature. This means that the flux from these panels is dominated by the correction which tends to destabilize the solver. However, increasing panel refinement to the order of the particle improves the fluxing to the surrounding flow.

The Nyquist instability is even more pronounced for a remeshed vortex method as compared to the vortex particle method. This is expected as the stair-step nature of surrounding particles is amplified on a Cartesian grid compared to the a vortex particle method where particles follow the contour of the body. Eldredge observed that using a refinement ratio of 3 removes this instantly.However, naturally in our case we use a panel refinement ratio of atleast 6 to damp the oscillations. As shown in the figure below, a panel refinement ratio of 1 induces severe noise in the impulse reflected in the lift and drag results. This can be compared to the panel ratio of $\frac{N_p h}{c} = 6$. The result shows that there is a drastic reduction in noise with increase in panel resolution.

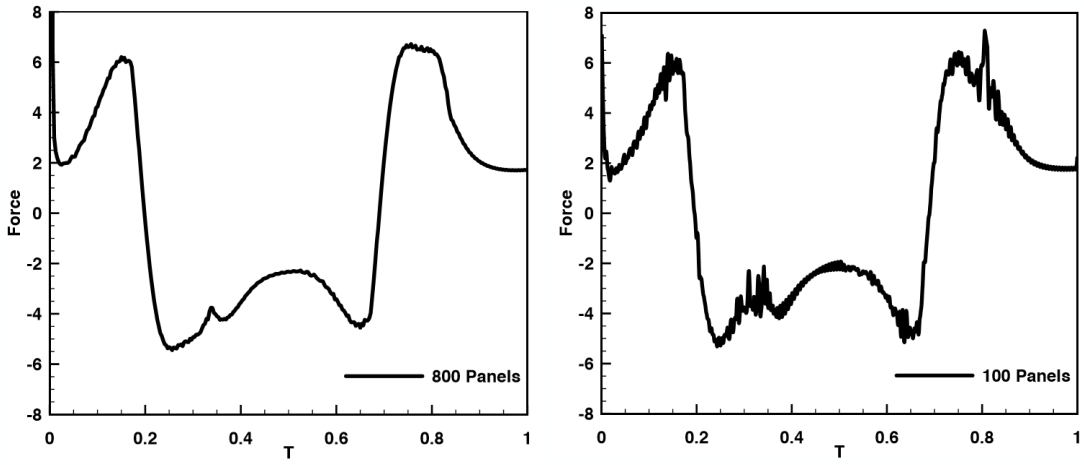

Figure 2.5: Drag and Lift Results form Vortex Particle method (a) Refinement ratio=2 (b) Refinement ratio=6 for an aspect ratio 1:5 flapping ellipse

2.10 Summary

The current chapter summarizes the method of applying the no slip boundary condition in Vortex Panel Method. This step is at the core of the Self Corrective Vortex Fluxing Method.

Chapter 3

Designing a Self Healing Solver

3.1 Motivation

In the previous chapter, a methodology to apply the no slip boundary condition and release vorticity into flow was discussed. By utilizing the Neumann Boundary condition for flux, instead of specifying $u.s = 0$ at boundary explicitly, the panel solver adds an extra step of indirection to ensuring no slip.

Studies by Marichal [16] and Eldredge [17] indicate that the fluxing method introduced by Komoutsakos shows first order convergence at the boundary in both no slip and no throughflow characteristics. This implies that in a typical vortex particle approach some throughflow error was achieved leading to possible vorticity leakage into the body.

Some treatment of this issue was proposed by Winckelmans [8] such that a potential correction was applied during the convection substep to minimize throughflow of vorticity in to the body. Surprisingly, no noticeable difference in force results was observed indicating a global conservation of flowfield characteristics being intrinsic to the panel method.

Yet this source of error has almost gone unnoticed in symmetric flows where such a potential correction scheme was not implemented [5][12] yet still reliably producing accurate flowfield and force characteristics. Ploumhans studied the application of symmetric redistribution scheme in a vortex particle method approach, thus deliberately leaking vorticity into the body every few timesteps. Again, no noticeable difference in flow characteristics was observed. These studies points towards an inherent self corrective aspect to vortex panel methods such that any spurious leakages into the body are fixed within the timestep.

This chapter studies the mechanism behind the vortex particle method approach and identifies the reasoning behind self correction. We also outline the formulation used to simulate all steps within the vortex in cell algorithm. This self correction is then coupled with our slip formulation to simulate highly asymmetric and wake re-entering body flows in chapter 4.

3.2 Vortex Particle Method Approach

The panel method introduced in the previous section was utilized in order to study inviscid flows. For a fully viscous simulation, the vortex particles must find a way to release from the surface and evolve independently within the fluid. The governing equation for incompressible two dimensional Navier Stokes

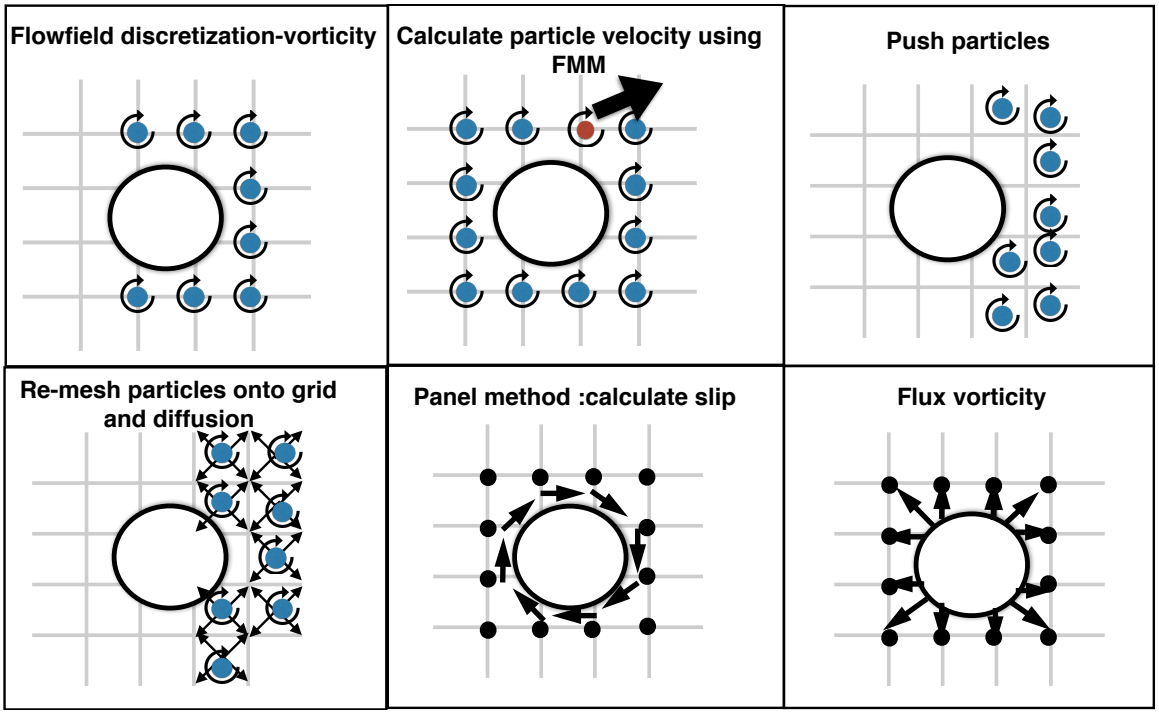

Figure 3.1: The naive vortex particle method approach

flow in vorticity-streamfunction formulation is:

$$\frac{\partial w}{\partial t} + (u.\nabla)\, w = (w.\nabla)\, u + v\Delta w \tag{3.1}$$

Where $w(x,t)$ is the vorticity at a location($\nabla \times u(x,t)$) and $u(x,t)$ refers to the velocity vector of the vortex particle. This equation is broken down into a fractional step algorithm .Thus the inviscid and viscous part of the simulation are completely split from each other.

Algorithm Description.

$$\frac{\gamma}{\Delta t} = -\frac{\partial \omega}{\partial n} \tag{3.2}$$

$$\frac{\partial \omega}{\partial t} = u.\Delta\omega \tag{3.3}$$

$$\frac{\partial w}{\partial t} = v\Delta w \tag{3.4}$$

$$\omega_p = \omega_M \tag{3.5}$$

$$\Gamma_{body} = \sum \omega_i h^2; \tag{3.6}$$

$$I = \sum \omega_i x_i \tag{3.7}$$

$$\frac{\partial w}{\partial t} = v\Delta w \tag{3.8}$$

$$(X_b, V_b, t + dt)^{n+1} = K(X_b, V_b, t) \tag{3.9}$$

$$\omega = \omega_M - \omega_{body} \tag{3.10}$$

$$F = \frac{dI}{dt} \tag{3.11}$$

1. **Convection** The convection substep solves the inviscid potential flow equation. We wish to solve the Poisson's equation , given an unbounded vorticity distribution, for the streamfunction at each point in the domain.

$$\Delta\psi = -\omega(x) \tag{3.12}$$

The solution of this equation can be obtained bu solving for the Green's function for an impulsive vortex source.

$$\Delta\psi = -\delta(x - x') \tag{3.13}$$

The resulting impulse response known as Green's function is the solution to the Laplace equation:

$$G(x, x') = \frac{1}{2\pi} Log\,(x - x') \tag{3.14}$$

The actual streamfunction can then be derived by superposing the actual finite vorticity flow field with

the Greens function.

$$\psi_{\Omega}(x) = \frac{1}{2\pi} \int_{V} Log\,(x - x')w(x')dx' \tag{3.15}$$

The curl of this streamfunction gives the resultant velocity at a point in the flowfield:

$$U_w = \nabla \mathrm{x} \int_{V} G(x, x')\omega(x')dV \tag{3.16}$$

In the case of a body being present within the flowfield, the net velocity at a point includes both flowfield and body influences represented as:

$$U = U_w + U_s + U_\gamma + U_\infty \tag{3.17}$$

Where $U(x,t)$ is the velocity induced at the particle. U_w is the influence of all vortex particles in the fluid calculated as per equation(6).

U_γ represents the vortex sheet influence on the vortex field. Since the vortex sheet is non existent at this substep, this component is equated to zero. U_b is the influence of the body vorticity on the flowfield. In the case of a uniformly rotating body Komoutsakos [5] shows the body can be replaced by a uniform vorticity source of vortex strength equal to twice the angular velocity.

$$\psi_{\Omega} = -\frac{\Omega(t)}{\pi} \int_{V} Log\,(x - x')dx' \tag{3.18}$$

Here Ω represents the angular velocity and ψ_Ω represents the streamfunction due to rotation. This can be used to calculated the velocity field component due to rotation as follows:

$$U_{\Omega} = \nabla \times \psi_{\Omega} \tag{3.19}$$

This volume integral component can be converted to a surface integral over the surface of the body as proved in Appendix A. Extending this approach to a general moving body, vortex and source sheets on body surface can be used to represent arbitrary deformations and rotations. However in this case, the influence of each panel differs depending on the local body velocity at the point. The influence of body in this case can be represented as:

$$u_s = \oint \nabla G(x, x')\mathrm{x}(\mathrm{n}'\mathrm{x}u_b(\mathrm{x}'))\mathrm{dS} - \oint \nabla G(x, x')(\mathrm{n}'.u_b(\mathrm{x}'))\mathrm{dS} \tag{3.20}$$

This formulation is intuitive as the first component includes the influence of the rotational velocity at the body surface modelled as a vortex source. The second term models the influence of the deformation velocity as a source local to each panel. In case, the body is under pure rotation, the body influence devolves to its volume integral form in (3) and (4).

This velocity is calculated by superimposing the influence of all influences at the grid point. We exclude the influence of a particle upon itself in this calculation. Each particle is then displaced to its new location based on forward timestepping.

The Biot Savart calculation is a naive approach with cost $O(N^2)$. However the process can be significantly speeded up by application of Fast Multipole Method which reduces the computational cost to $O(N \log(N))$.

2. **Remeshing**

   Once the particles are displaced by convection from their original location, they are no longer on the grid. Particles not placed on a grid pose two problems. (i) Continued advection of particles leads to clustering of vortices in some areas and depletion in others causing the well known phenomenon of Lagrangian distortion.[12] This causes a decrease in accuracy of solution as particles become so close to each other that their induced velocity on each other becomes aphysically large. (ii) Particles not on a grid require more computationally expensive integral operators such as Particle Strength Exchange tracking in order to find and track their nearest neighbours within a viscous radius. Moreover, if particles are not superimposed ontop a grid, each iteration leads to creation of new particles which grows exponentially with time and a careful trimming criteria must be used to decide which particles to keep. By keeping all particles on a grid, we circumvent the need for particle tracking. Thus we remesh the particles onto the grid at each iteration after the convection substep. This maintains accuracy and The particles are then interpolated back onto the grid using remeshing. In this work we have utillized the M4 symmetric kernel given by Komoutsakos [5] which conserves the first four moments of vorticity.

3. **Diffusion** All preceding steps model the flowfield as inviscid potential flow which conserves the vorticity of each vortex element. However, in a real flow the vorticity of each particle is exchanged and diffused to surrounding particles. Moreover, vorticity enters the flow from the boundary layer present over the body. Eldredge and Komoutsakos utilize Particle Strength Exchange to exchange vorticity between particles which is applicable to vortex particle methods.The current work utilizes a vortex in cell method poses the advatange that all points lie on the grid at each time step. Thus diffusion is carried out using a second order Runge Kutta finite difference Scheme over a cartesian grid. The resulting

operation on each grid point can be shown as:

$$\frac{\partial w}{\partial t} = v\Delta w \tag{3.21}$$

4. **Flushing Out Vorticity from within the Body**

   Once, the impulse of the vorticity field has been computed the vorticity inside the body must be removed. As shown in equation 3.10 we record the total circulation inside the body that will be fluxed out at the next timestep and flush vorticity within half a cell spacing h of the body. The necessity of flushing vorticity within this envelope is to prevent singularities in velocity induced as particles approach the panel surface too closely.

5. **Measurement of Forces on a Body**

   The computation of forces induced on the body are computed at each time step using the impulse formulation given as:

$$F = \frac{dI}{dt} + \frac{d}{dt}\int_{\mathrm{A}} u_b dA \tag{3.22}$$

   (a) **Previous Surface force Formulation**

   This computation is carried out by third order backward finite difference operator. This formulation relies on computation of volume integrations over the domain and body. Previous methodologies such as [1] and [2] have used a surface formulation of the above equation for force calculation. Zhang [18] used the following formulation:

$$F = -\rho_f \oint\!\!\!\!\!\!\diagup_{A_f} \left[(x - X_c) \times \left(\frac{d\omega}{dn}\right) + vn \times \omega + (x - X_c) \times n \times \frac{du_b}{dt}\right] ds \tag{3.23}$$

   The first two terms represent the influence of vorticity within the flow whereas the last term is the force contribution of the body kinematics . The first term represents the physical flux from the body at the current timestep which is already known while applying the no slip condition. It is also an indirect measurement of surface pressure as shown in the previous chapter. Naturally this term is highly oscillatory, as the vorticity streamfunction formulation is designed to eliminate pressure from calculation.

   The advantages of this force method are that , there are no volume integrals of vorticity within the body. This is advantageous from the point of view of deforming body kinematics where internal

velocity is not known apriori.

Numerical studies revealed that the flux term is highly oscillatory while moving the body through the grid. This is because Ploumhans [3] and Komoutsakos [4] have shown that surface forces rely on measurement of vorticity flux that is essentially highly dependent on surrounding particles close to the body. Moreover, the second term represents the viscous force on surface contribution, found by twice differentiating the streamfunction over the body. This approach was previously attempted by Ploumhans and the twice differentiation leads to significant oscillations of body attached vorticity close to the surface.

(b) **Current Volume-Surface based Force formulation** It is possible to maintain the surface kinematics advantage of the previous formulation while also avoiding local surface based oscillations in force. An alternate formulation represents the contribution from the surface force as a volume integral. This is in the spirit of the corrective nature of vortex fluxing method. While no special treatment used at wall might change the vorticity locally, the overall flowfield is conserved over timesteps. By splitting the surface velocity contribution from the vorticity contribution we arrive at an alternative formulation.

$$F = -\rho_f \oint_{A_f} \left[(x - X_c) \times \left(\frac{d\omega}{dt} \right) + (x - X_c) \times n \times \frac{du_b}{dt} \right] ds \tag{3.24}$$

We thus retain the volume based integral of force calculation over the fluid domain while retaining the surface integral for the body induced forces in the second term. In the case of a rigid body, this integral can be reexpressed as a global volume integral since the vorticity inside the body is just twice the angular rotation rate.

$$F = -\rho_f \frac{d}{dt} \int_{A_f} (x \times \omega) dV + \rho A_b \frac{dU}{dt} - 2\rho A_b \frac{d}{dt} (X_c \times \Omega) \tag{3.25}$$

Here Ω is the angular rotation rate the given timestep. We use formulation 3.24 for evaluating forces on deforming bodies whereas equation 3.25 is used for all our rigid body force calculations. In later sections, we will expand on why this formulation gives accurate results for our solution as opposed to the local surface based formulation to preserve the nil special treatment advantage.

3.3 Derivation of Equations

While we analysed the slip equation in the previous chapter and briefly mentioned the contributions in the equation 3.17 , the mathematical formulation for these contributing terms is yet to be derived. This section starts by arriving at a formulation for our no slip equation.

Using Maxwell's reciprocity and the symmetry of the green's function we can represent the influence of deformations inside the body in the form of internal vorticity of the body.This formulation was presented by Chatelain. [19]

$$u_b = \int_V \nabla_x G(x,x') \times \omega(x') dx' = -\int_V \nabla_{x'} \times (G(x,x')\omega(x'))dx' + \int_V G(x,x')(\nabla_{x'} \times \omega(x'))dx' \quad (3.26)$$

$$u_b = \int_S (G(x,x')\omega(x')) \times n(x')dx' + \int_V G(x,x')(\nabla_{x'} \times \omega(x'))dx' \quad (3.27)$$

$$\nabla \times \nabla \times u = \nabla(\nabla.u) - \nabla^2 u \quad (3.28)$$

$$u_b(x) = \int_S (G(x,x')\omega(x')) \times n(x')dx' - \int_S (\nabla^2_{x'} G(x,x')u_i(x'))dx' + \int_S (\nabla_{x'} G(x,x')u_i(x')) - (G(x,x')\nabla_{x'} u_i(x')).n(x')dx' \quad (3.29)$$

In the above equation we have ignored the contribution of non divergence free sources within the body by assuming

$$\nabla.u_b = 0 \quad (3.30)$$

While this assumption is reasonable Gazzola et al [1] have shown this term can have significant contribution to the swimming forces on a deforming body. Here the second term goes to zero as the dirac delta term is evaluated to zero everywhere outside the body.

$$n \times (\nabla \times u) + n.\nabla u = n.(\nabla u)^T \quad (3.31)$$

$$(\nabla u)^T = \left(\frac{\partial u_j}{\partial u_i}\right) \quad (3.32)$$

Switching to tensor notation:

$$\int_V \frac{\partial}{\partial x_j}\left(\frac{\partial u_j}{\partial u_i}G\right)dx = \int_V \frac{\partial^2}{\partial x_i \partial x_j}(u_j G) - \frac{\partial}{\partial x_j}\left(u_j \frac{\partial G}{\partial x_i}\right)dx = \int_V \frac{\partial}{\partial x_i}\left(\frac{\partial u_j}{\partial x_j}G + u_j\frac{\partial G}{\partial x_j}\right)dx - \int_V \frac{\partial}{\partial x_j}\left(u_j\frac{\partial G}{\partial x_i}\right)dx \tag{3.33}$$

$$\int_V \frac{\partial}{\partial x_j}\left(\frac{\partial u_j}{\partial u_i}G\right)dx = -\int_S (n_i u_j \frac{\partial G}{\partial x_j} + n_j u_j \frac{\partial G}{\partial x_i})dx \tag{3.34}$$

$$u_s = \int_S (\nabla_x G(x,x') \times (n \times u(x')) - \int_S (\nabla_x G(x,x')(n.u(x')))dx \tag{3.35}$$

At this point, we superimpose the contributions of the body deformations to all other contributions. The boundary slip equation can be obtained at each point on the surface. The velocity field on the surface **below** the surface of the vortex sheet but **above** the surface of body is given as:

$$u = \int_{V_{fluid}} \nabla G(x,x') \times \omega(\mathrm{x}')\mathrm{dV} + \frac{(n \times \gamma)}{2} + \oint_{Panels} \nabla G(x,x') \times \gamma(\mathrm{x}')\mathrm{ds} + \frac{1}{2}u_b + u_s + U_\infty \tag{3.36}$$

The vortex sheet can be related to the surface velocity using the following tangential velocity condition called no slip.

$$u.\tau = u_b.\tau \tag{3.37}$$

In order to solve for no slip we have to account for not only the jump due to the vortex sheet but also due to the now singular body contribution.

Using eq 3.36 and eq 3.37 by taking a cross product with the normal vector we get:

$$\frac{-\gamma}{2} + n \times \int \nabla G \times \gamma ds + \frac{n \times u_b}{2} + n \times \int \nabla G \times \omega(x')dx' + n \times u_s = n \times u_b \tag{3.38}$$

Which simplifies to:

$$-\frac{\gamma}{2} + n \times \int \nabla G \times \gamma ds = -\left(\frac{-n \times u_b}{2} - \int \nabla G \times \omega(x')dx' - n \times u_s\right) \tag{3.39}$$

Our derivation differs from the approach mentioned by Eldredge in that we solve for no slip between the body and the vortex sheet in eq . The previous formulation solves for no slip below the surface of

the body. The final formulation is shown below as:

$$-\frac{\gamma}{2} + n \times \int \nabla G \times \gamma ds = -\left(\frac{n \times u_b}{2} - \int \nabla G \times \omega(x')dx' - u_s\right) \times n + U_{body} \tag{3.40}$$

Here U_{body} represents the influence of the movement of the centroid of the moving body analogous to a translating body or a body in freestream. In the case of a rigid non rotating body U_{body} is the only active term in our version of the slip equation.

6. **Boundary condition enforcement of no slip** In the last section, we arrived at our formulation for the no slip equation.We summarize the usage of this formulation to complete the vortex particle methodology. At the end of the convection and diffusion , a non zero slip velocity exists on the surface of the panels that must be cancelled. Komoutsakos modelled this approach using the vortex fluxing panel method. The surface is discretized into line segments called panels. The vortex particle field creates a spurious slip velocity on the surface of each panel. An infinitely thin vortex sheet is attached to each panel on the surface of the body to cancel the slip velocity underneath them.

   The velocity at a point at the no slip substep can be represented as:

$$u(x) = \int\limits_{V_{fluid}} \nabla G(x, x') \times \omega(\mathrm{x}')\mathrm{dV} + \oint\limits_{Panels} \nabla G(x, x')\mathrm{x}\gamma(\mathrm{x}')\mathrm{ds} + u_s + U_\infty \tag{3.41}$$

   Where the second term is the U_γ vortex sheet panels influence on each other and U_b denotes the body influence given by (10). As the panel is approached from inside the body, the velocity inside the body becomes the local body velocity u_b measured at each collocation point. The panel and body influence subsequently break into two parts:the influence of other panels at a collocation point and a panel's own induced velocity below itself.

$$u_b = \int\limits_{V_{fluid}} \nabla G(x, x') \times \omega(\mathrm{x}')\mathrm{dV} + \frac{(n \times \gamma)}{2} + \oint\limits_{Panels} \nabla G(x, x') \times \gamma(\mathrm{x}')\mathrm{ds} + \frac{1}{2}u_b + u_s + U_\infty \tag{3.42}$$

   This is the Friedholm's integral equation of the second kind for the general deofrming/rotating body. It is solved by inverting a linear system of N+1 equations for N unknown vortex sheet strengths using a minimal least squares method. The extra equation comes from vorticity conservation by Kelvin Circulation Theorem.

   This vortex sheet is then diffused from each panel using the diffusion scheme introduced by Ploumhans [3] for a general geometry. This is represented by the diffusion of vorticity flux into the flow field:

$$\frac{\gamma}{\Delta t} = -\frac{\partial \omega}{\partial n} \tag{3.43}$$

Here γ refers to the vortex sheet strength of the selected panel. Once the vortex sheet strength is fluxed into the flowfield, no slip is achieved. We utilize Ploumhan's general fluxing scheme as it doesnt require the particles to lie on a body conforming grid and works well on a regular Cartesian grid as shown in [3]. This was done to preserve the nil special treatment advantage of the panel method.

3.4 Self correction abilty of Vortex Panel method

All of the above substeps except the no slip application are done unaware of the body location or orientation. This introduces aphysical leakage of vorticity fluxing into the body during the convection, diffusion and remeshing steps. Below we first analyze the influence of this leakage on a "naive" vortex particle solver unaware of these aphysical leaks. We then later introduce a small modification that gives allows the vortex method to self correct these leaks on its own to design a "self corrective" solver.

1. **The naive vortex method approach**

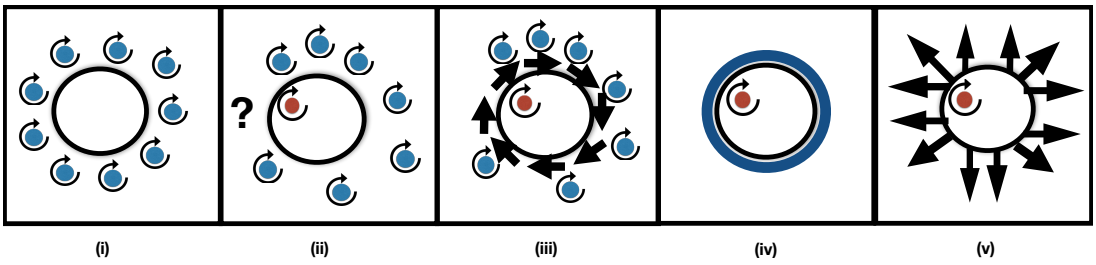

Figure 3.2: The naive vortex particle method approach

This process is shown in the above figure where vorticity leaks into the body and interferes with the solution within the flowfield. The detailed steps on the effects of this interference are outlined below:

Step(i) vorticity leaks into the body by virtue of remeshing,convection or dIffusion.

Step(ii) Not only is the vorticity at the location missing but the vorticity entering inside the body contributes to the slip from inside the body by reversing induced velocity contribution.

Step(iii) This slip contribution cannot be cancelled by the vortex sheet properly leading to improper satisfaction of no slip boundary condition. Due to the **Linked Kinematic Boundary condition** no throughflow is only satisfied as accurately as no slip and thus more particles leak into the body at the next timestep.

Step(iv) The extra vorticity leaking into the body causes the vortex sheets to overcompensate and end up with higher aphysical strengths to cancel the slip induced by vorticity internal to the body .

Step (v) :These stronger vortex sheets in turn are shed into the flow through the Neumann boundary condition and increase slip on the surface in step.

2. **The self corrective vortex method approach** We base our self corrective solver design on an

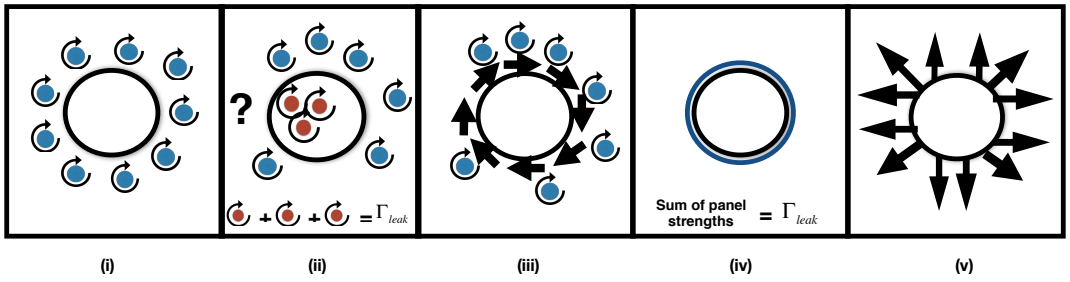

Figure 3.3: The self corrective vortex method procedure

intuitive mathematical explanation:

While analyzing the Panel method in chapter 2 , the no slip equation was applied in **??** to solve for the vortex sheet strengths.

$$u_{body} = u_{slip} + u_b - \frac{\gamma(s)}{2} \oint_{Body} K \times \gamma(s) ds \tag{3.44}$$

In the above equation u_{slip} refers to external vortex particles influence on the vortex sheet strength. **Thus the sheet strength is proportional to the magnitude of slip induced at the surface.**

(i)Vorticity shed from the body is designed to cancel slip at the neighbouring body location.

(ii)Any loss of vorticity from a point close to the body into the body, induces an excess slip at the body panel locally with the particles no longer present in vicinity to cancel it.

A modification to the Kelvin Circulation theorem can also account for the lost circulation into the body as follows.

$$\Gamma_{correction} = \Gamma_{rot} + \Gamma_{leak} \tag{3.45}$$

Here Γ_{leak} is the cumulative sum of all leaked vorticity into the body. This formulation was previously introduced by Eldredge [6] to account for minor leaks during remeshing substep every five timesteps, while resorting to special treatment to prevent diffusion and convective leakage.

Since slip is analogous to a vortex sheet formation on the boundary as in 3.44, a vortex sheet of more than usual strength is created at the panel which fluxes to restore the vorticity at its original lost location.The excess strength comes from the reservoir of leaked vorticity. In light of this discussion we demonstrate below how this self correction procedure works.

Step(i): The vorticity around the body moves and diffuses into the body.

Step(ii): The vorticity leaks into the body as expected however, we proceed with the modification in 3.45 to modify the slip equations solved by summing the circulation inside the body, irrespective of source of entry.

Step(iii): The vorticity is flushed from within $0.5h$ of the body and cumulative vorticty from outside the body is computed in additon to body influences. It is important to mention that force and impulse measurement must be done **prior** to this step and including the contribution of the leaked vorticity into the body.

Step(iv): The vortex particle method accurately replaces the lost vorticity to its original lost location and calculates the accurate vortex sheet strength.

Step(v): The vorticity is fluxed into the flow thus preserving total conservation of circulation.The particle method also corrects the flwo by restoring the vorticity lost at the last time step to its original ocation.

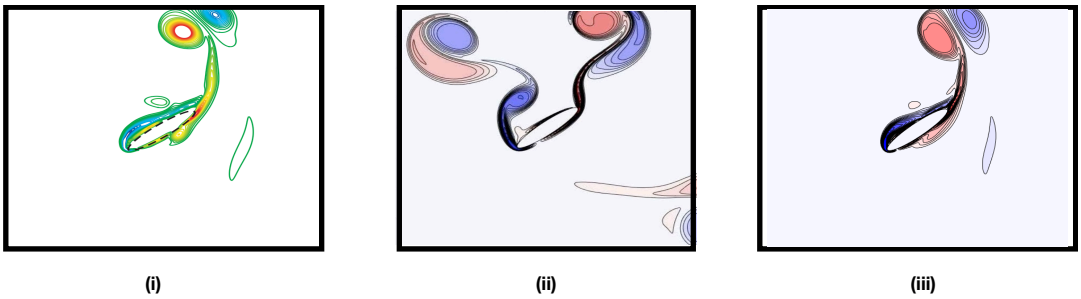

Figure 3.4: (i)The vorticity field reference solution of a dragonfly from Eldredge (ii) The naive approach solution (iii)The solution using modification of Kelvin circulation theorem

The figure above shows a typical simulation and compares the true solution obtained by special treatment in (i) with the body unaware method using the naive approach (ii) and the modified self correcting approach (iii). The self corrected approach clearly matches the vorticity contours of the actual result.

All previous approaches have been cautious in letting vorticity leak into the body leading to careful treatment of flow at the walls. To prevent this spurious flux leakage from happening several approaches have been

attempted in literature. Ploumhans [3] and Lonfils [20] create mirror images of vorticity inside the body during diffusion to disable reverse flux. Ploumhans also reflects any vortex particle getting too close to the body that induces noise in the solution.
In vortex particle approaches by Eldredge arrange a fresh layer of zero strength particles fitted around the body every time the flow is remeshed within 4-5 time steps with a specific trimming criteria to ensure zero strenght particles around the body.

Our methodology is advantageous from the standpoint of a flow solver as we dont need to use special treatments in the form of biased kernels close to the body fo any step.Thus all calculations can easily be done on a standard Cartesian grid using symmetric diffusion and remeshing stencils. Moreover,any convective leakages are corrected by the algorithm leading to significantly highter timesteps than comparble methodsl ike the Brinkmann Penalization method.

3.5 Summary

We conclude this section by discussing the key features of our implementation of a self corrective vortex in cell method.
(i) We first examined the vorticity-streamfunction formulation of the Navier Stokes equations and why they prove to be advantageous in their compact nature and large timesteps.
(ii)The convection, diffusion and remeshing schemes were then discussed.
(iii) The novelty in the current study lies in testing and stretching the hypothesis that the panel method regenerates any vorticity lost into the body with a few important modifications.
(iv)Our method differs from previous implementations by **eliminating all wall-based special treatment from any steps within the solver and relying completely on the abilty of the fluxing to correct the resulting spurious vorticity leakages** .
(iv) This proves advantageous as compared to previous approaches as we use symmetric stencils for remeshing, diffusion and a standard cartesian grid.
(v)This approach enhances the robustness and flexibility of the vortex particle method approach.
The concluding chapter explores the validity of this physical explanation by testing the self correction aspect of the panel method to its limit for symmetric and highly asymmetric flows.

Chapter 4

Results and Discussion

This chapter focuses on the validation of the self corrective vortex method. We discuss the accuracy of results obtained with our self correcting solver and introduce gradually severe test cases for both rigid and deforming bodies. The testcases are intentionally picked to validate our hypothesis about the self correction of all spurious leakages of vorticity into a body.

We first study symmetric flow test cases for flow past a rigid cylinder at Reynolds number 40,550 and 1000. Next we look at asymmetric flow test cases,particularily those that test the hypothesis of self correction to the limit. Natural test cases falling into this category include flapping wings moving within their own wake.

Finally we look at deforming bodies to ensure that our methodology works for deforming bodies as well as rigid bodies. We conclude by presenting our results for a deforming fish-shape figure exhibiting carangiform mechanics. Unless mentioned otherwise, for the force measurement the lift and drag coefficients are normalized as follows:

$$C_L = \frac{2F_y}{\rho U^2 c} \tag{4.1}$$

$$C_D = \frac{2F_x}{\rho U^2 c} \tag{4.2}$$

For the remainder of this chapter, red and blue vorticity contours denote anti clockwise and clockwise direction of rotation respectively.

4.1 Flow past Impulsively started Cylinder at Re 40

The first test case studied is the flow past an impulsively started Cylinder at Reynolds Number 40. This testcase was the starting point of the vortex method, with extensive validation given by Komoutsakos [5] and Leonard vis-a-vis the analytical solution and other numerical methods [3]. Komoutsakos utillizes a body fitted polar grid with biased remeshing stencils close to the wall. Unlike the previous method however,our

method applies symmetric (body-unaware) stencils close to the body and the body is placed on a regular cartesian grid. Thus it is important to compare how the current vortex fluxing methodology compares to solvers with special treatment at the walls.

The highly viscous flow regime also means there is substantial flux of vorticity into the body during the diffusion substep. The solution differs at the first few time steps from the Particle method and the analytical

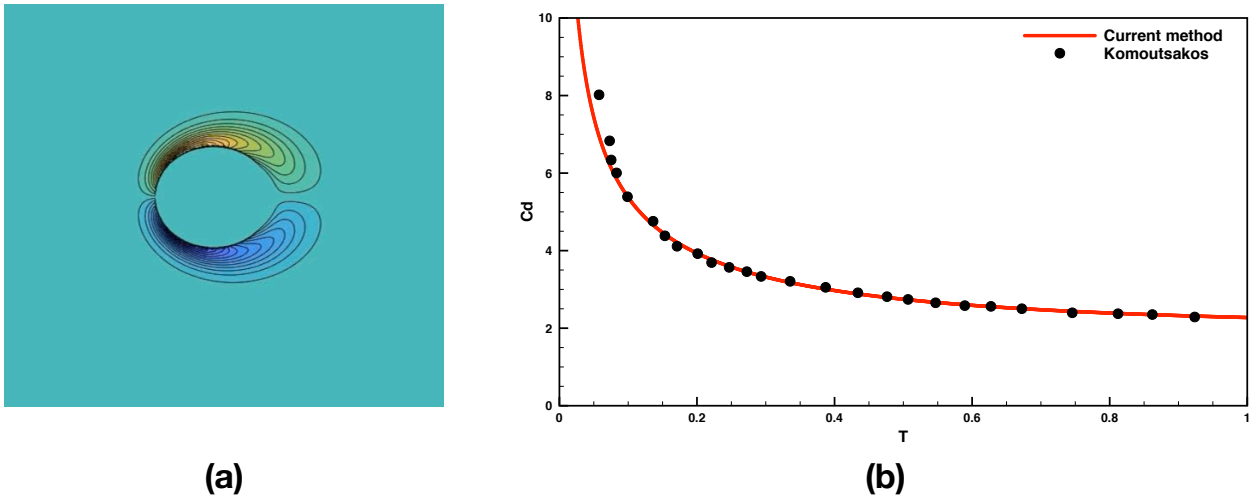

Figure 4.1: Flow Past cylinder Reynolds number 40 with vorticity contours at T=3 **(i)** and Drag comparision with Komoutsakos Body Fitted Particle method **(ii)**

solution and matches well after $T > 0.05$. As an impulsive start is not possible,the deviation can be explained as initially the vorticity created by an impulsive start exceeeds the Lagrangian CFL limit locally close to the body $\frac{\omega h^2}{v} >> 1$. At later timestep this condition is satisfied again and hence the solution regains accuracy. The parameters used for the Re 40 simulation are given below:

Table 4.1: Flow past Re 40 Cylinder

Symbol	Parameter name	Value
Re	Reynolds Number	40
U	Freestream Velocity	1
R	Radius	1
D_{diff}	Diffusion Parameter	1.05
X	Domain Size in X	[-4,4]
Y	Domain Size in Y	[-4,4]
R_p	Refinement Ratio	1
h	Grid Spacing	0.01
dt	Timestep	0.0025

4.2 Flow Past Impulsively Started Cylinder at Re 550

We extend our study to another comparision with two different vortex particle method solvers developed based on the work by Komoutsakos.

The first solver used for comparison,developed by Kim [21] explicitly uses mirror imaging of vortex particles at the boundary during Particle Strength Exchange to prevent an aphysical vorticity flux into the body. This step has also been used by Lomfils and Ploumhans in their vortex particle method.

The second particle method is the Ploumhans particle method solver used for vorticity flowfield comparision. The Ploumhans particle method utillizes additional special treatment in the form reflection of particles close to the boundary thus "bouncing" them back into the flow. This approach was observed to induce noise in the forces on the body. The drag characteristics of our solver along with a Vortex Lagrangian Particle Solver given by Kim[5] and corresponding experimental results are plotted in figure 4.2. We obtained a more accurate match with the experimental results.

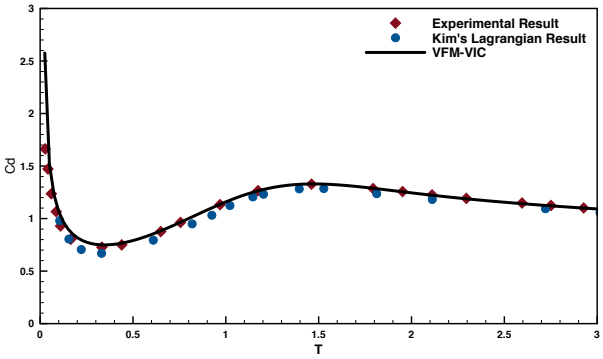

Figure 4.2: Flow Past cylinder with Reynolds number 550 dRwith vorticity contours at T=3 **(i)** and Drag comparision with Komoutsakos Body Fitted Particle method **(ii)**

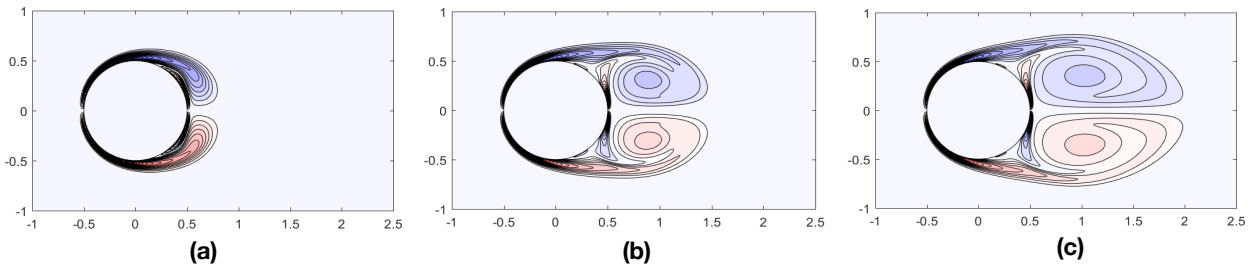

Figure 4.3: Vorticity contours obtained by current methodology (Left) **T=1** (Middle) **T=3** (Right) **T=5**

The vorticity contours with those presented by Ploumhans particle method are compared [7]. The

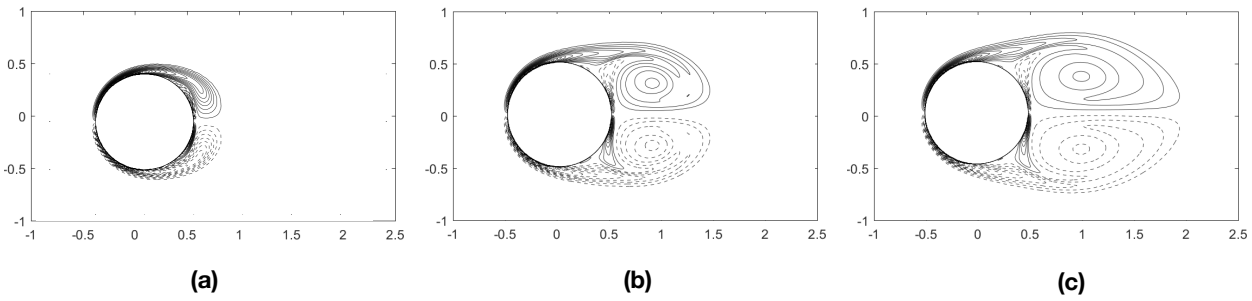

Figure 4.4: Vorticity contours obtained by Ploumhans particle method (Left) **T=1** (Middle) **T=3** (Right) **T=5**

vorticity contours are plotted in steps of 2 between -60 and 60 with zero contour ommited. A good qualitative match is obtained between the vorticity contours showing that the scheme introduced works well in replicating essential flow features.

Table 4.2: Flow past Re 550 Cylinder

Symbol	Parameter name	Value
Re	Reynolds Number	550
U	Freestream Velocity	1
R	Radius	1
D_{diff}	Diffusion Parameter	1.00
X	Domain Size in X	[-4,4]
Y	Domain Size in Y	[-4,4]
R_p	Refinement Ratio	2.5
h	Grid Spacing	0.01
dt	Timestep	0.01375

In light of the above observations,this case study indicates that removal of complex special treatment at boundary and instead relying on self correction can lead to equally accurate results vis-a-vis sophisticated vortex particle methods.

4.3 Flow over Moving Cylinder at Reynolds Number 1000

We study the flow past an Impulsively started Cylinder at Reynolds Number 1000 and ocmpare results with the Penalization Solver,both in terms of accuracy and numerical parameters including mesh resolution and timestep. This testcase presents an interesting comparision with the penalization solver as the timestep goes up with it. We use the same parameters as Case 2. The primary parameter to note is the $\frac{\Delta x^2}{4\nu t}$. The diffusion ratio controls the fluxing of the vorticity form the panels to the surrounding flow. Too small a value leads to vorticity being artificially confined close to the body leading to unstable divergence. Whereas a large value implies vorticity being diffused away too quickly from the boundary layer. This parameter is kept at 1.1

for all our simulations. This proves to be a within the range given by Eldredge 0.25-1.15 albeit towards the higher side.

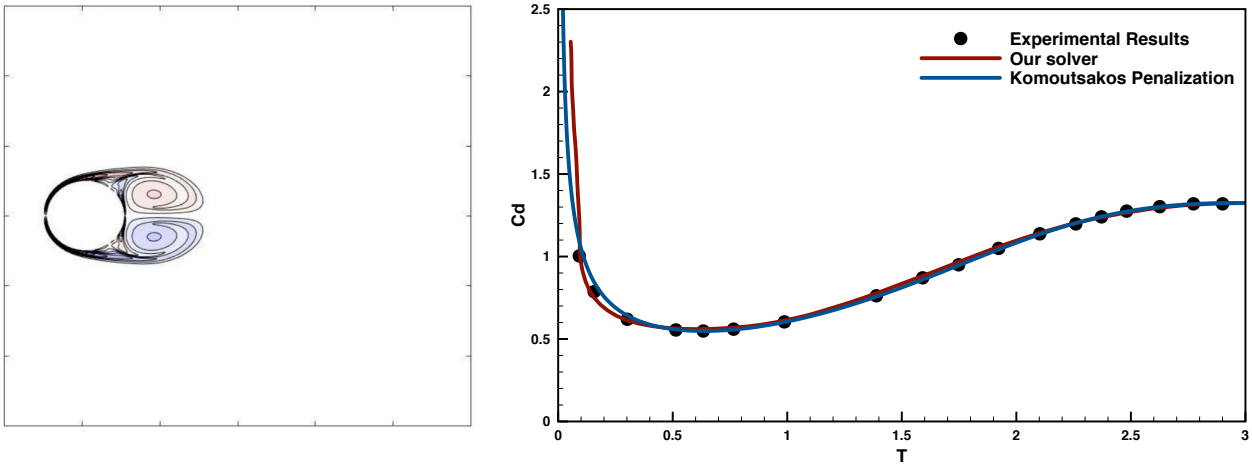

Figure 4.5: Flow Past cylinder Reynolds number 1000 with vorticity contours at T=3 **(i)** and Drag comparision with Penalization method **(ii)**

Table 4.3: Flow over Re 1000 moving Cylinder

Symbol	Parameter name	Value
Re	Reynolds Number	1000
U	Freestream Velocity	1
R	Radius	1
D_{diff}	Diffusion Parameter	1.00
X	Domain Size in X	[-4,4]
Y	Domain Size in Y	[-4,4]
R_p	Refinement Ratio	4.0
h	Grid Spacing	0.01
dt	Timestep	0.025

An advantage posed by the current method is that it scales with Reynolds number. The timestep and mesh resolution 0.0125 and 0.01 respectively used in the current method are whereas the timestep and resolution used in the other are (1e-5) and (2.5e-2) respectively. While Penalization methods utilize forcing to add vorticity into the flow as a byproduct,panel methods deal with fluxing the natural vorticity smoothly to surrounding flow leading to the above mentioned significantly more relaxed requirements in timestep.

4.4 Flow induced in quiescent fluid by Dragonfly wing

The previous cases have analysed the self corrective nature of the panel method from the perspective of a symmetric flow. In this case an equal amount of positive and negative vorticity leaks into the body. We now

test the solver with a severe asymmetric flow test case. A flapping wing that is both translating and rotating through a quiescent fluid is a motion where non zero vorticity leaks into the body. The spurious vorticity flux exacerbated by the thinness of the body being unable to rigidly impose no throughflow. It is desirable to test this self corrective hypothesis in the case of a body moving in and out of its wake,thus consuming a significant portion of its vorticity by virtue of its motion. We validate using the same kinematics given in Case 1 by [17]. We compare the vorticity contours with those given in [17] in figure 4.4.

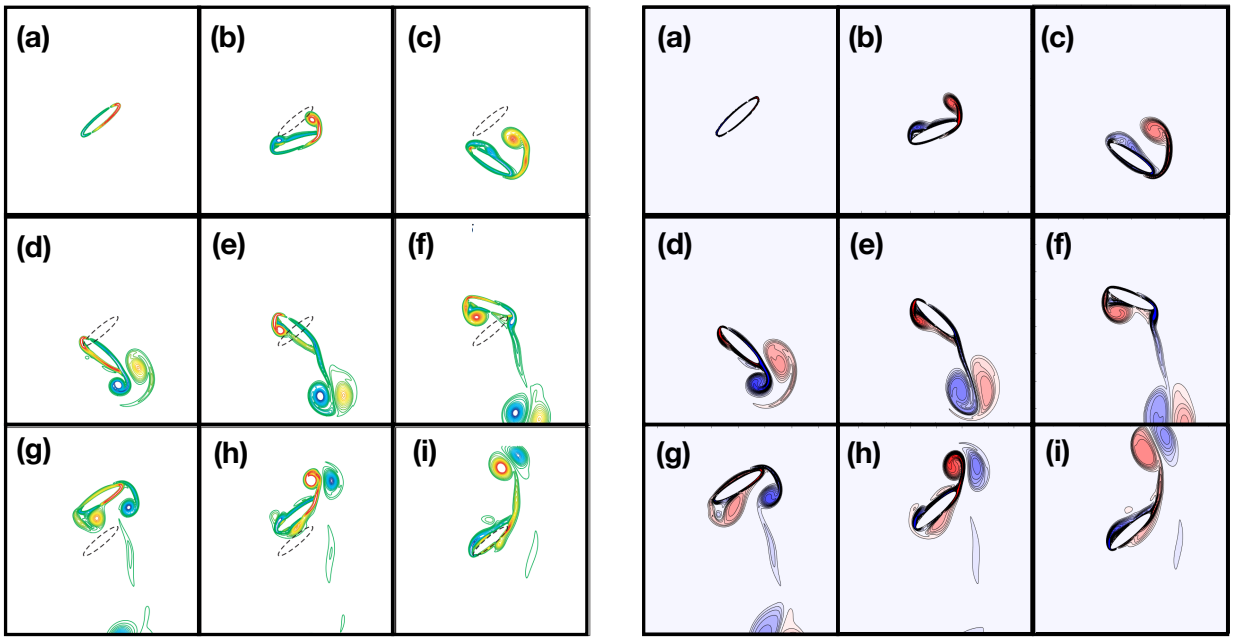

Figure 4.6: (Left) vorticity contours of dragonfly as shown by Eldredge (Right) vorticity contours given by current method at times

The vorticity contours shown are at time (a) T=0, (b) T=0.125, (c) T=0.25, (d) T=0.375 (e) T=0.5 (f) T=0.625 (g) T=0.75 (h) T=0.875 (i) T=1 . An accurate qualitative comparison is obtained in the locations of major vortex structures when compared to the particle method. Conservation and regeneration of vortex structures is further reinforced in the lift and drag characteristics obtained in figure 4.4. Here,we only plot the fluid forces thus removing the imposed body dependent components that are independent of fluid kinematics. The fluid forces are thus solely dependent on the time derivative of impulse imparted to the fluid. The vertical and horizontal impulse is explicitly dependent on the spatial location of the vorticity and its magnitude. The accurate match in lift and drag forces confirms that not only is the correct amount of vorticity conserved in the fluid but its x and y locations in the form of impulse are also maintained.
An important observation in the current methodology is that increase in refinement of panels for a given grid spacing reduced the noise in the results. A typical panelling ratio required for non noisy solution is $R_p = 4$.

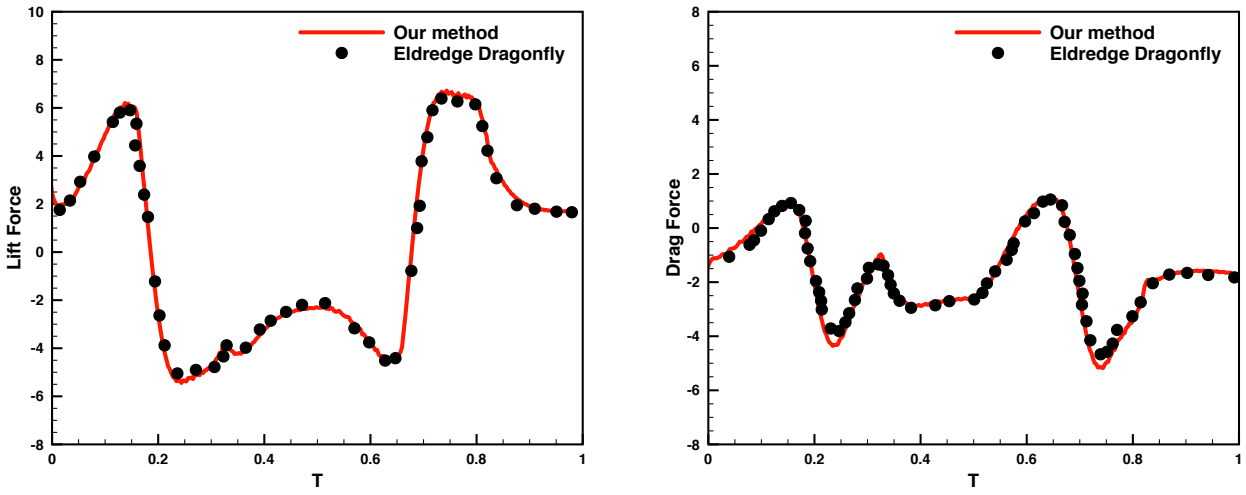

Figure 4.7: (Left)Lift force comparison with Eldredge Dragonfly and Drag comparison with Eldredge Dragonfly **(ii)**

Table 4.4: Dragonfly Wing

Symbol	Parameter name	Value
Re	Reynolds Number	550
St	Strouhal Number	0.25
c	Major Axis Chord length	1
AR	Aspect Ratio	0.2
X	Domain Size in X	-4,4
Y	Domain Size in Y	[-4,4]
N_p	Number of Panels	800
h	Grid Spacing	0.01
dt	Timestep	0.0125
Δt_t	Direction change interval	0.667T
Δt_r	Incidence Angle change interval	0.333T
Δt_{lag}	Direction Change lag from Peak Pitch	0.08T
α	Incidence Angle Amplitude	40 deg

This panelling ratio proved to be higher than observed by Eldredge ($R_p = 1.5$) which can be explained .The noise created is likely due to the circulation distribution by panels in areas of high curvature leading to a significant component going to the correction. While Eldredge uses a fresh layer of body fitted particles around the body,the cartesian grid is more liable to this noise in high curvature regions as the grid follows the body in a highly stairstep configuration. A vortex particle method however has particles following the contour of the body except for the reshing step every 4-5 iterations. Thus noise is amplified .This explains why a higher panellnig ratio was used in our simulations using 276 panels.

4.5 Deforming Cylinder at Reynolds Number 100

We consider the case of a deforming cylinder to validate our self corrective methodology for deforming bodies. The cylinder periodically deforms into an ellipse shape such that total area is preserved.

We compare our results with those presented by Zhang [18] . The results presented compare the vorticity contours and the radial velocity profiles for the given case Re_Ω=100 at timesteps T=8.25,8.5,8.75,9 in the case of a radially deforming cylinder. As shown in the figure,a symmetry is observed in the induced vortex structures around the body which are a good match to the Eldredge particle scheme. The previous methodology applied a shrinking and expanding domain size closely following the boundary layer. However,previous simulations showed that vorticity generated by the deforming cylinder is quickly nullified by counter rotating vortices before diffusing outwards and thus a small domain size was picked.

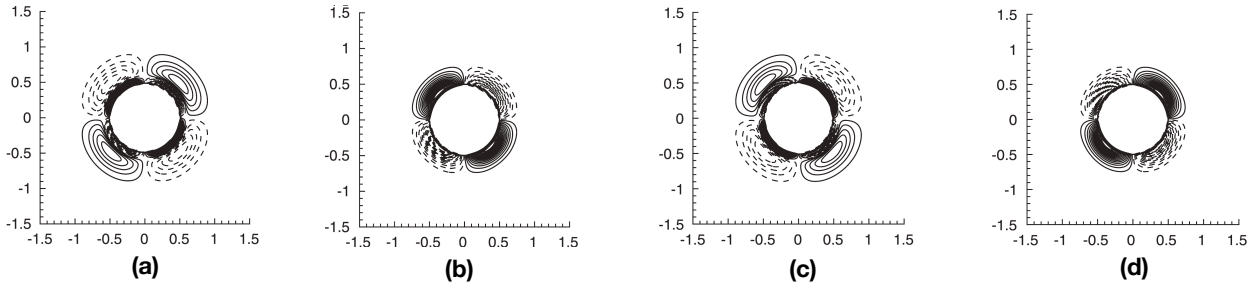

Figure 4.8: Vorticity contours formed over radially deforming cylinder at $Re_\Omega = 100$ **(a)** T=8.25 **(b)** T=8.5 **(c)** T=8.75 **(d)** T=9 given by Zhang

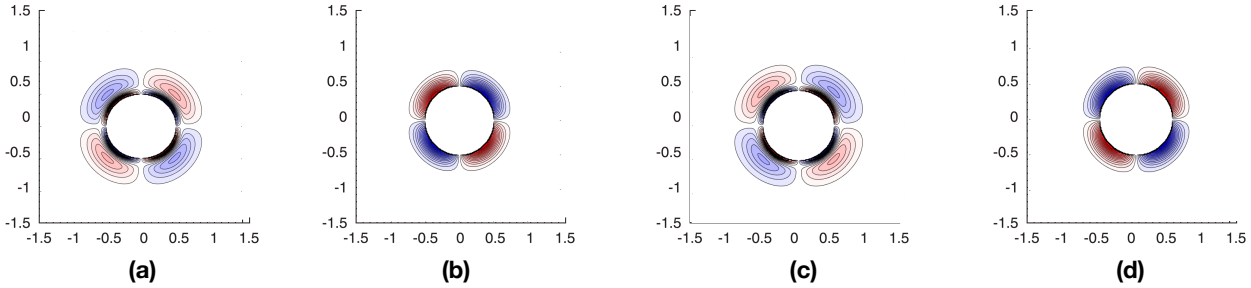

Figure 4.9: Vorticity contours formed over radially deforming cylinder at $Re_\Omega = 100$ **(a)** T=8.25 **(b)** T=8.5 **(c)** T=8.75 **(d)** T=9 using current method

The vorticity contours clearly match with our body unaware interpolation method. This points towards the viabilty of the method towards both rigid and deforming bodies. The body formulation used to solve for panel strength slightly differs from the previous implementation and is given in the Appendix . A validation of the radial velocity profiles is also given in figure 4.5. No noticeable differences were observed in

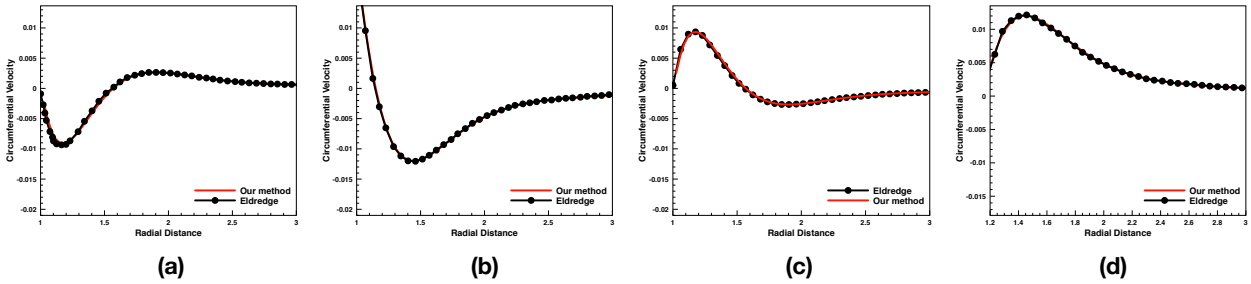

Figure 4.10: Circumferential velocity comparision along 45 degree line over radially deforming cylinder at $Re_\Omega = 100$ **(a)** T=8.25 **(b)** T=8.5 **(c)** T=8.75 **(d)** T=9 using current method.Data: Our method (red line) ,Eldredge Particle method (dotted black line)

Table 4.5: Deforming Cylinder Re 100

Symbol	Parameter name	Value
Re_Ω	Oscillation Reynolds Number	100
Ω	Deformation Frequency	1
R	Radius	1
a_o	Deformation Amplitude	0.02
X	Domain Size in X	[-3,3]
Y	Domain Size in Y	[-3,3]
N_p	Number of Panels	400
h	Grid Spacing	0.02
dt	Timestep	0.00275

the circumferential velocity comparision vis-a-vis the Eldredge formulation results. We obtain an accurate flowfield and velocity comparision despite the fact that particles were arranged on a polar grid around the body in the Eldredge formulation.

4.6 Deforming Cylinder at Reynolds Number 500

We present another deforming cylinder comparision of our methodology with the Zhang-Eldredge formulation based on two new key points. We validate the accuracy and abilty of our methodology in capturing an increasingly thin boundary layer in response to increasing the Reynolds number but keeping our resolution constant from the previous case. Moreover, it was also important to validate the radial velocity characteristics which depend heavily on the deformation term within our formulation. Interestingly,unlike the previous case where circumferential velocity matched those obtained by Eldredge,noticeable differences in the radial and circumferential velocity were observed between analytical,current method and previous formulation results. The vorticity contours are presented in figure 4.6.

Despite the lack of resolution(the oscillation amplitude is equivalent to the grid resolution h) we observe a good match with the results by Eldredge in the thin boundary layer region. We wish to also validate the

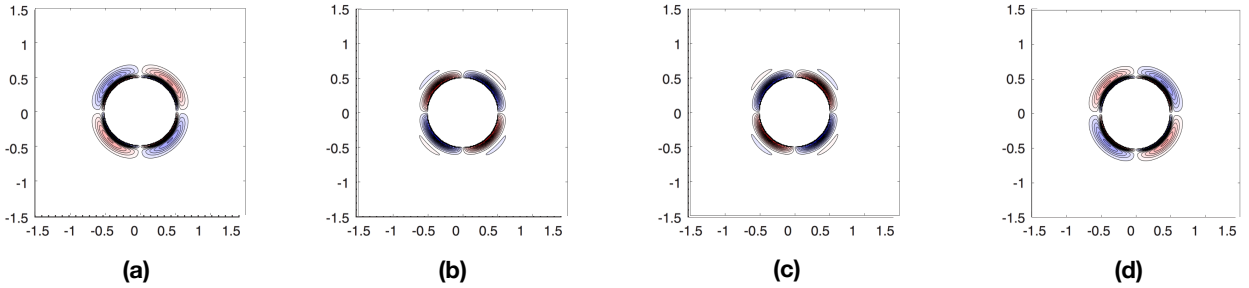

Figure 4.11: Vorticity contours formed over radially deforming cylinder at $Re_\Omega = 500$ **(a)** T=8.25 **(b)** T=8.5 **(c)** T=8.75 **(d)** T=9 using current method

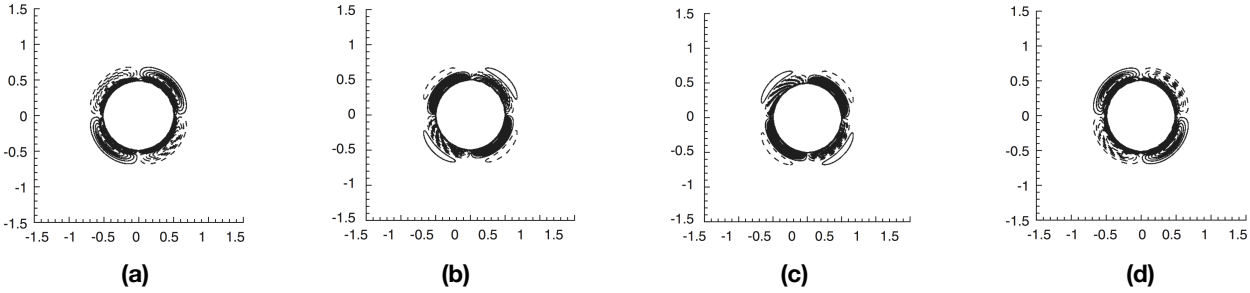

Figure 4.12: Vorticity contours formed over radially deforming cylinder at $Re_\Omega = 100$ **(a)** T=8.25 **(b)** T=8.5 **(c)** T=8.75 **(d)** T=9 given by Zhang

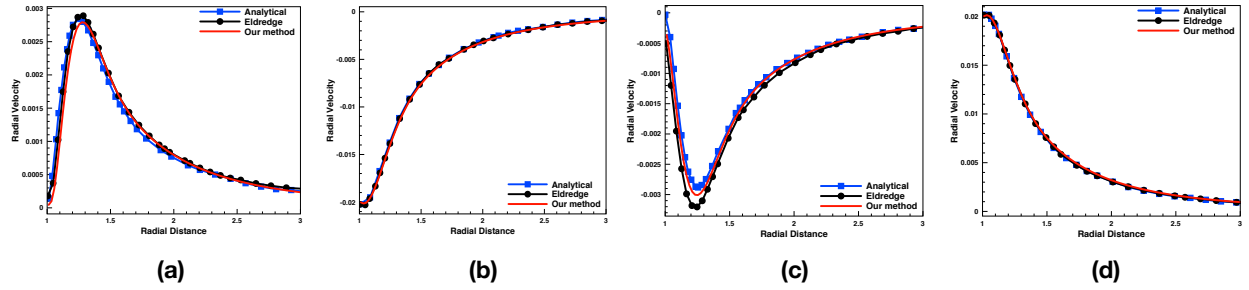

Figure 4.13: Radial velocity comparison along 0 degree line over radially deforming cylinder at $Re_\Omega = 500$ **(a)** T=8.25 **(b)** T=8.5 **(c)** T=8.75 **(d)** T=9 using current method.Data: Our method (red line) ,Eldredge Particle method (dotted black line) ,Analytical result(squared blue line)

radial velocity along the positive 0 deg axis to confirm the validity of the deformation term in our formulation. Figure 4.6 shows that overall the current methodology more accurately matches the analytical result for all timesteps. A similar observation in the circumferential velocity induced at positive 45 deg is observed. The difference is more noticeable in both of the above cases for T=8.25 AND t=8.75. We observe that not only does the current method replicate accurate results while using coarse resolution,it also provides a slightly better match to analytical results.

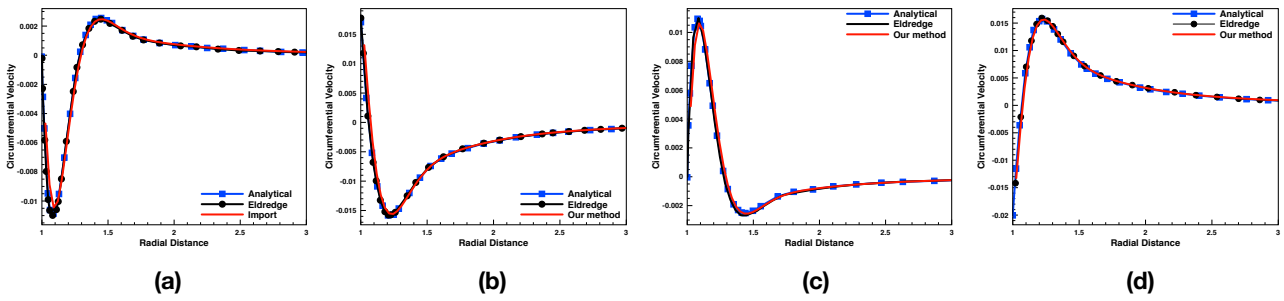

Figure 4.14: Circumferential velocity comparision along 45 degree line over radially deforming cylinder at $Re_\Omega = 500$ **(a)** T=8.25 **(b)** T=8.5 **(c)** T=8.75 **(d)** T=9 using current method.Data: Our method (red line) ,Eldredge Particle method (dotted black line) ,Analytical result(squared blue line)

Table 4.6: Deforming Cylinder Re 500

Symbol	Parameter name	Value
Re_Ω	Oscillation Reynolds Number	500
Ω	Deformation Frequency	1
R	Radius	1
a_o	Deformation Amplitude	0.02
X	Domain Size in X	-4,4
Y	Domain Size in Y	[-4,4]
N_p	Number of Panels	400
h	Grid Spacing	0.02
dt	Timestep	0.011

4.7 Flow over a rapidly rotating fruitfly wing in quiescent fluid

At this point we wished to further validate our formulation for the slip equation for rotating body. In contrast to the previous case however,the rotation rate for a fruitfly is significantly larger(almost instantaneous) . Moreover, we switch towards a lower Reynolds regime and a thinner aspect ratio than the dragonfly case to study flow past a fruitfly wing. In order to do so the aspect ratio used was 10:1 for a unit chord ellipse flapping and pitching in a quiescent fluid. Due to the thinness, throughflow error is exacerbated and the body moves through its own wake similar to the previous case. The vorticity contours for the fruit fly are shown below. We modify the lift and drag force measurements in line with data comparison.

$$C_L = \frac{2F_y}{\rho {U_{max}}^2 c} \tag{4.3}$$

$$C_D = sign(U)\frac{2F_x}{\rho {U_{\max}}^2 c} \tag{4.4}$$

The fruitfly rapidly rotates and moves into its wake testing the self correction abilty of the vortex particle

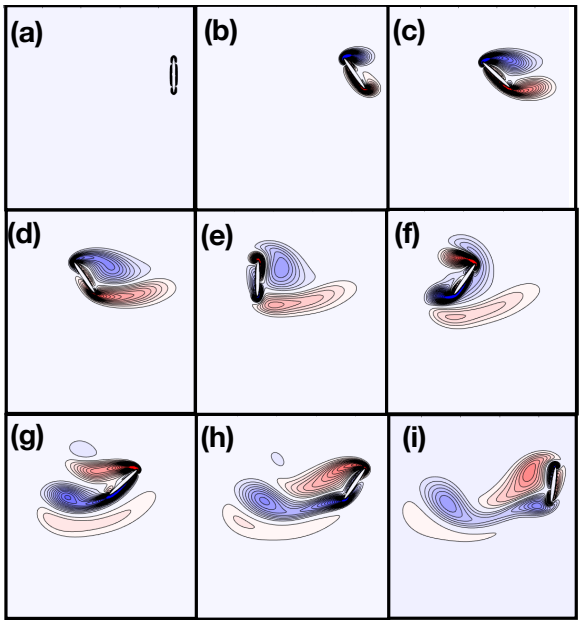

Figure 4.15: Vorticity contours given by current method for Re 75, St=0.25 flapping fruitfly elliptical wing

method significantly. This is also reflected in the lift and drag curves that show the vortex method conserves the global vorticity flowfield.

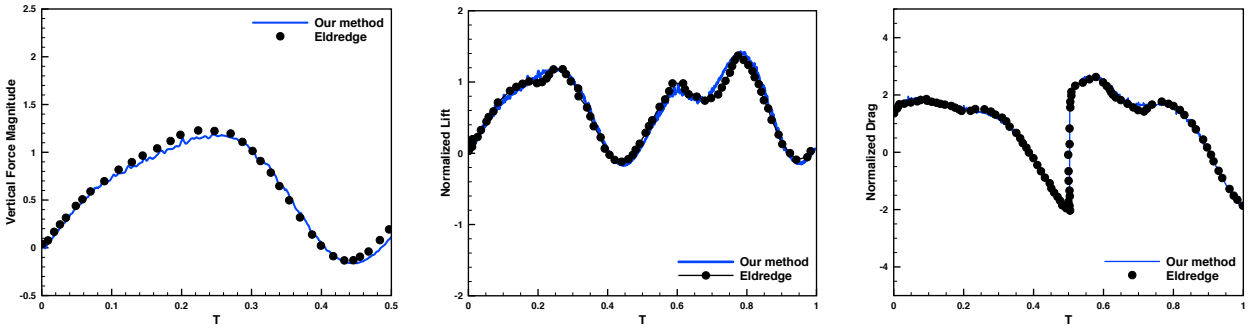

Figure 4.16: (Left)Vertical force comparison with Eldredge Dragonfly (Center) Normalized Lift force comparison (Right) Normalized Drag force comparison, Data: Eldredge Particle Method(black dots) Current method (Blue Line)

The results shown above can be explained as follows. The first Figure shows the unscaled lift force compared with Eldredge's methodology. The same results are shown in Fig where the normalized Lift Coefficient is compared between the two methodologies.

We normalize the results with the mean lift over a cycle. While all three data comparisions were done from study given in [6] it was found that the normalized lift coefficient was inconsistent with the data in the same data given for the unscaled values. To avoid any discrepancy all three results are plotted in Fig 4.7.

Table 4.7: Re 75 Fruitfly

Symbol	Parameter name	Value
Re	Reynolds Number	75
St	Strouhal Number	0.25
c	Major Axis Chord length	1
AR	Aspect Ratio	0.1
X	Domain Size in X	-4,4
Y	Domain Size in Y	[-4,4]
N_p	Number of Panels	800
h	Grid Spacing	0.01
dt	Timestep	0.001875
α_o	Initial Incidence Angle	90 deg
β	Rotational amplitude	45 deg
A_o	Translational amplitude	2.8

An accurate match is obtained in the lift and drag forces thus validating our formulation.

4.8 Flow past a deforming Insect Wing at Re 100

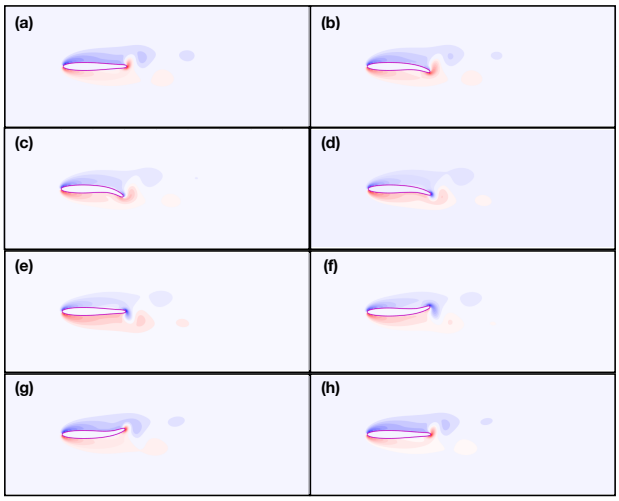

Figure 4.17: Vorticity contours for flow past deforming insect wing at Re 100

We now extend the current methodology to flow past a deforming structure similar to an insect wing. The body kinematics imposed are symmetric by design to detect any signs of asymmetry in shed vortex structures without introducing a disturbance. These asymmetries if detected, would stem from the Kelvin circulation correction at each time step. The vorticity contours in figure 4.8 shown are at time (a) T=3, (b) T=3.125, (c) T=3.25, (d) T=3.375 (e) T=3.5 (f) T=3.625 (g) T=3.75 (h) T=3.875 (i) T=4 .

We observe that vortex structures obtained at the tail of the wing are mirror images across the horizontal x axis at time T=3.25 and 3.75. The large vortex structures shed at T=3.5 and T=4 also represent mirror images in terms of vorticity magnitude. The circulation conservation despite body unaware interpolation

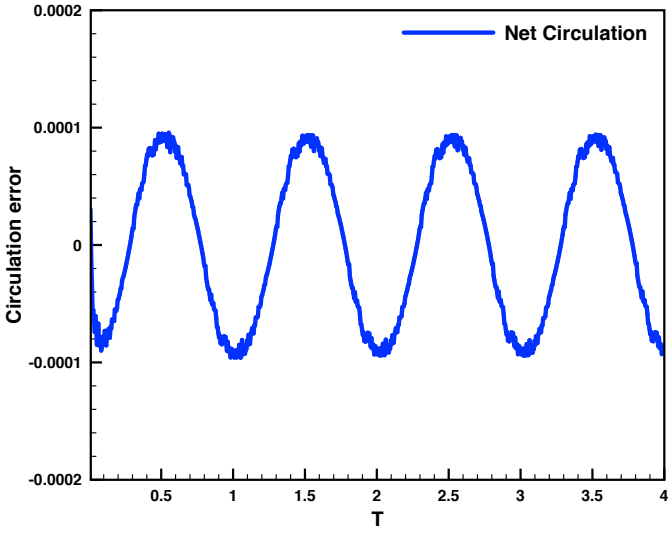

Figure 4.18: Kelvin circulation error in insect wing simulation

schemes is reestablished. This is further reinforced in the error remaining bounded to $1e^{-4}$ in circulation conservation shown in the figure 4.18.

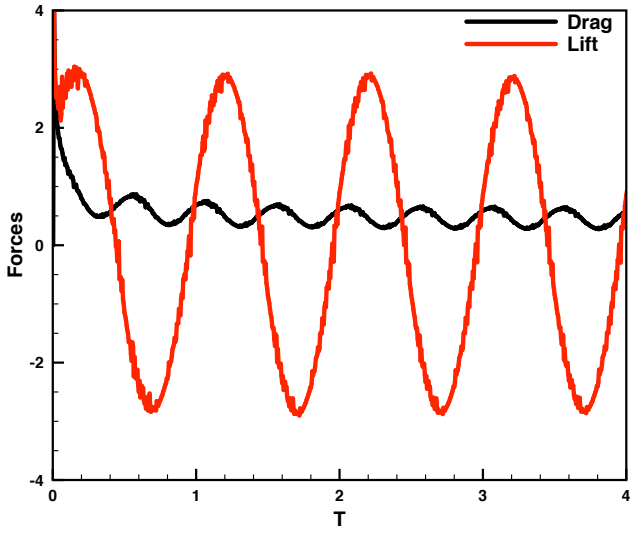

Figure 4.19: Lift and Drag Forces for insect wing

Table 4.8: Deforming Wing Re 100

Symbol	Parameter name	Value
Re	Reynolds Number	100
T	Time period	1
X	Domain Size in X	[-4,4]
Y	Domain Size in Y	[-4,4]
N_p	Number of Panels	900
h	Grid Spacing	0.01
dt	Timestep	0.0025

We now turn towards the drag and lift coefficient shown by current methodology using 3.24 including both fluid forces. This segment shows that the solver is capable of simulating deforming bodies.

Chapter 5

Conclusion and Recommendations

5.1 Discussion of Conclusions

The goal of this thesis was to develop an alternative vortex method solver that relaxes the severe timestep constraints of the Brinkmann Penalization solver while preserving its robustness and flexibilty to general bodies. For achieving this objective,the inspiration came from the vortex particle method which relaxes the timestep to the LCFL constraint. However additional requirements for the solver were that it must be robust and flexible and not subject to time consuming special treatment at the boundary .These were problems that restricted the usage of vortex particle methods. The special treatment techniques used in previous techniques can be classified as follows:

- A mesh grid conforming to a body fitted grid or arrangement of particles following the shape of the body . Such an approach is not extendable to a general deforming body.
- Particle imaging close to wall boundary to prevent diffusion based flux of vorticity into the body.
- Reflection of particles getting too close to the body. This methodology induces aphysical features in the force characteristics.
- One sided or biased interpolation diffusion and remeshing stencils close to the wall boundary.

Our methodology eliminates **all the above** artificial and inflexible treatments from the vortex particle method completely. The current method utilizes non symmetric (body-unaware) stencils for diffusion and remeshing of vortex particles on a standard Cartesian Grid.
The intuition behind eliminating these geometry-dependent treatments was based on the fluxing mechanism at the core of the particle method. Vortex particles fluxed into the flow are by design distributed to cancel the slip at the wall. Any loss of vortex particles into the body by avoiding special treatment induces an excess slip on the body panels. Since slip is represented as a vortex sheet on the surface of the body,this excess vorticity is later fluxed back into the fluid,thus restoring any lost vorticity at the boundary.

Once aware of this self corrective nature,we introduced simple but significant modifications to the boundary condition to preserve circulation. Next we tested the hypothesis of self correction for rigid rotating and deforming bodies by comparing our results with special treatment solvers in severe test cases.The severity of test cases was determined by rapid rates of rotation, thinness of body and objects moving into their own wake,thus significantly absorbing their self generated vorticity and testing the self correction ability to its limits.

Finally our goal was achieved by designing a solver that preserves the large timestep advantage of the particle solver while removing any close-to-wall special treatments enhancing its robustness and applicability to a general geometry.

5.2 Recommendations

Our recommendations for future work to improve upon the current solver are submitted below:

1. **Mollified Boundary:** The panel method being a sharp interface method induces subgrid oscillations in the force characteristics. These oscillations were found undesirable form a standpoint of self propulsion. To eliminate these oscillations some form of "mollification" of boundary is desirable. A deliberate mollification of panel boundary to match grid resolution as introduced by Kim [21] can be expected to control these oscillations.

2. **Higher order Panel method:** The convergence of panel method to improve accuracy to third order can be attempted by following the methodology for an inviscid panel method given by Kuzmina [22] for computing the vortex sheet strengths and then releasing them into the flow using the fluxing methodology.,Kuzmina et al utilize analytically integrated computationally inexpensive formulations to eliminate any singular kernels due to proximity of vortex sources to the boundary.

3. **A Hybrid Brinkmann-Penalization and Fluxing method solver**: Once the fluxing substep is applied, a small penalization over a mollified boundary using the Brinkmann step can not only elminate residual slip and throughflow errors but also cub these oscillations. By working concurrently with the fluxing method,the forcing caused by Penalization is reduced,thus preserving the timestep advantage.More importantly,the vortex method is more susceptible to noise in high curvature regions,something unobserved in Penalization methods simulating C-start configurations to fishes. [23]. The panels must maintain "a line of sight" for flux to reach sufficient particles which diminishes in

regions of high curvature surrounded by a cartesian grid. The optimal combination of the two methodologies can further overcome each of their shortcomings.

4. **Spectral decomposition:** By spectral decomposition of the Friedholm equation of second kind,applied during the no slip step can lead to a more stable vortex sheet computation. The singularity induced due to the thinness of body caused by panels coming together can be removed. This approach presented by Komoutsakos [5] requires an extension to a non elliptical general deforming body.

References

[1] M. Gazzola, P. Chatelain, W. M. Van Rees, and P. Koumoutsakos, "Simulations of single and multiple swimmers with non-divergence free deforming geometries," *Journal of Computational Physics*, vol. 230, no. 19, pp. 7093–7114, 2011.

[2] S. Verma, G. Abbati, G. Novati, and P. Koumoutsakos, "Computing the force distribution on the surface of complex, deforming geometries using vortex methods and brinkman penalization," *International Journal for Numerical Methods in Fluids*, vol. 85, no. 8, pp. 484–501, 2017.

[3] P. Ploumhans and G. Winckelmans, "Vortex methods for high-resolution simulations of viscous flow past bluff bodies of general geometry," *Journal of Computational Physics*, vol. 165, no. 2, pp. 354–406, 2000.

[4] P. Koumoutsakos and A. Leonard, "High-resolution simulations of the flow around an impulsively started cylinder using vortex methods," *Journal of Fluid Mechanics*, vol. 296, pp. 1–38, 1995.

[5] P. Koumoutsakos, A. Leonard, and F. Pepin, "Boundary conditions for viscous vortex methods," *Journal of Computational Physics*, vol. 113, no. 1, pp. 52–61, 1994.

[6] J. D. Eldredge, "Numerical simulation of the fluid dynamics of 2d rigid body motion with the vortex particle method," *Journal of Computational Physics*, vol. 221, no. 2, pp. 626–648, 2007.

[7] P. Ploumhans, G. Winckelmans, J. K. Salmon, A. Leonard, and M. Warren, "Vortex methods for direct numerical simulation of three-dimensional bluff body flows: application to the sphere at re= 300, 500, and 1000," *Journal of Computational Physics*, vol. 178, no. 2, pp. 427–463, 2002.

[8] G.-H. Cottet and P. Poncet, "Advances in direct numerical simulations of 3d wall-bounded flows by vortex-in-cell methods," *Journal of Computational Physics*, vol. 193, no. 1, pp. 136–158, 2004.

[9] J. Katz and A. Plotkin, *Low-speed aerodynamics*, vol. 13. Cambridge university press, 2001.

[10] P. R. Spalart, "Vortex methods for separated flows," 1988.

[11] C. Cooper and L. Barba, "Panel-free boundary conditions for viscous vortex methods," in *19th AIAA Computational Fluid Dynamics*, p. 3546, 2009.

[12] F. Pepin, "Simulation of the flow past an impulsively started cylinder using a discrete vortex method," tech. rep., California Institute of Technology Pasadena Graduate Aeronautical Labs, 1990.

[13] L. Manickathan and A. Palha, *Hybrid Eulerian-Lagrangian vortex particle method*. PhD thesis, Ph. D. thesis, Delft University of Technology, 2015.

[14] A. J. Chorin, "Numerical study of slightly viscous flow," *Journal of Fluid Mechanics*, vol. 57, no. 4, pp. 785–796, 1973.

[15] L. Greengard and V. Rokhlin, "A fast algorithm for particle simulations," *Journal of computational physics*, vol. 73, no. 2, pp. 325–348, 1987.

[16] Y. Marichal, "An immersed interface vortex particle-mesh method," *Universit Catholique de Louvain*, 2014.

[17] J. Eldredge, "Efficient tools for the simulation of flapping wing flows," in *43rd AIAA Aerospace Sciences Meeting and Exhibit*, p. 85, 2005.

[18] L. J. Zhang and J. D. Eldredge, "A viscous vortex particle method for deforming bodies with application to biolocomotion," *International journal for numerical methods in fluids*, vol. 59, no. 12, pp. 1299–1320, 2009.

[19] P. Chatelain, *Contributions to the three-dimensional vortex element method and spinning bluff body flows*. 2005.

[20] T. Lonfils, *Numerical investigations of vortex systems: time-developing and space-developing simulations. Improvements of the vortex-in-cell method for external flows using both an immersed boundary approach and a multiple-space resolution technique*. PhD thesis, PhD thesis, Université catholique de Louvain, 2010.

[21] Y.-C. Kim, J.-C. Suh, and K.-J. Lee, "Vortex-in-cell method combined with a boundary element method for incompressible viscous flow analysis," *International Journal for Numerical Methods in Fluids*, vol. 69, no. 10, pp. 1567–1583, 2012.

[22] K. Kuzmina, I. Marchevskii, and V. Moreva, "Vortex sheet intensity computation in incompressible flow simulation around an airfoil by using vortex methods," *Mathematical Models and Computer Simulations*, vol. 10, no. 3, pp. 276–287, 2018.

[23] M. Gazzola, W. M. Van Rees, and P. Koumoutsakos, "C-start: optimal start of larval fish," *Journal of Fluid Mechanics*, vol. 698, pp. 5–18, 2012.